Optimizing Four Years of CO_2 Biospheric Fluxes from OCO-2 and in situ data in TM5 : Fire Emissions from GFED and Inferred from MOPITT CO data

Hélène Peiro [1], Sean Crowell [1], and Berrien Moore III [1]

[1]University of Oklahoma, Norman, OK, USA

Correspondence: Helene Peiro (helene.peiro@ou.edu)

Abstract. Column mixing ratio of carbon dioxide (CO_2) data alone do not provide enough information for source attribution. Carbon monoxide (CO) is a product of inefficient combustion often used as a tracer of co-emitted with CO_2. CO data can then provide a powerful constraint on fire emissions, supporting more accurate estimation of biospheric CO_2 fluxes. In this framework and using the chemistry transport model TM5, a CO inversion using MOPITT v8 data is performed to estimate fire emissions which are then converted in CO_2 fire emissions (called FIREMo) through the use of emission ratio. These CO_2 fire emissions allow us, then, to estimate adjusted CO_2 Net Ecosystem Exchange (NEE) and respiration which are then used as priors for CO_2 inversions constrained either by the Orbiting Carbon Observatory 2 (OCO-2) v9 or by in situ data. These optimized CO_2 fire emissions (FIREMo) are used to re-balance the CO_2 Net Ecosystem Exchange (NEEmo) and respiration (Rmo) with the global CO_2 growth rate. Subsequently, in a second step, these rebalanced fluxes are used as priors for a CO_2 inversion to derive the NEE and ocean fluxes constrained either by the Orbiting Carbon Observatory 2 (OCO-2) v9 or by in situ CO_2 data. For comparison purpose, we also balanced the respiration using fire emissions from the Global Fire Database Emissions (GFED) version 3 (GFED3) and version 4.1s (GFED4.1s). We hence study the impact of CO fire emissions in our CO_2 inversions at global, latitudinal and regional scales over the period 2015 - 2018 and compare our results to the two other similar approaches using GFED3 FIRE3 and GFED4.1s (FIRE4) fires, as well as with an inversion using both CASA-GFED3 NEE and GFED3 fire priors (priorCMS)fire and NEE priors. After comparison at the different scales, the inversions are evaluated against TCCON data. Comparison of the flux estimates show that at global scale posterior net flux estimates are more robust than the different prior flux estimates. However, at regional scale, we can observe differences in fire emissions among the priors, resulting in large adjustments in the Net Ecosystem Exchange (NEE) to match the fires and observations. Results show that variations in posterior flux are much smaller across different prior mean fluxes when compared with the data assimilated. However, at global scale and for most of the regions, while the net fluxes remain robust, we can observe differences in fire emissions among the priors, resulting in large adjustments in the Net Ecosystem Exchange (NEE) to match the fires and observations. Tropical flux estimates from in situ inversions are highly sensitive to the prior flux assumed, of which fires are a significant component. Slightly larger CO_2 net sources are observed when using GFED4.1s and MOPITT CO prior in CO_2 OCO-2 inversions than compared with the other priors, particularly during the 2015 El Niño event for most Tropical regions. Larger CO_2 net sources with MOPITT CO and GFED4.1s priors are also observed in Tropical Asia in CO_2 in situ inversions

than compared with the other priors during the 2015-2016 El Niño period and shows large net emissions than compared to OCO-2 inversions. Slightly larger net CO2 sources are derived with posterior fire emissions using either FIRE4 or FIREMo in the OCO-2 inversion, in particular for most Tropical regions during 2015 El Nino year. Similarly, larger net CO2 sources are also derived with posterior fire emissions in the in-situ data inversion for Tropical Asia. Evaluation with TCCON suggests that the re-balanced posterior simulated give biases and accuracy very close each other where biases have decreased and variability matches better the validation data than with the CASA-GFED3. Further work is needed to improve prior fluxes in Tropical regions where fires are a significant component. Evaluation with TCCON data shows lower biases with the three re-balanced priors than with the prior using CASA-GFED3. However, posteriors have average bias and scatter very close each other, making it difficult to conclude which simulation is better than the other. One major conclusion from this work is the strong constrain at global scale of the data assimilated compared to the fire prior used. But results in the tropical regions suggest sensitivity to the fire prior for both the IS and OCO-2 inversions. Further work is needed to improve prior fluxes in tropical regions where fires are a significant component. Finally, even if the inversions using the FIREMO prior did enhance the biases over some TCCON sites, it is not the case for the globe. This study consequently push forward the development of a CO-CO2 joint inversion with multi-observations for possible stronger constraint in posterior CO2 fire and biospheric emissions.

1 Introduction

Carbon dioxide (CO_2) is the most important greenhouse gas contributing to global climate change (IPCC2014). Gaps in our understanding of the processes that control land-sea-atmosphere exchange of CO_2 are a leading order uncertainty in future projections of the global climate (Friedlingstein2014). The global net flux, and hence the airborne fraction, can be deduced from the atmospheric growth rate (Ballantyne2012), and historically different efforts, such as the Global Carbon Project (Le-Quere2009) have divided the total global net flux into its constituent components, consisting of fluxes from the ocean, terrestrial biosphere, fossil fuel combustion and other anthropogenic activities, and biomass burning.

CO_2 emissions from fires are well-characterized at the largest space and time scales, but the uncertainties increase rapidly as we look to finer space and time scales. Two approaches are currently employed to estimate global emissions from fires. The first uses, since 2017, total fuel consumption per product of the burned area and the fuel consumption per unit area deduced from the burned area and active fires products of the Moderate Resolution Imaging Spectroradiometer (MODIS). Previous years were based directly on burned area datasets. The Global Fire Emissions Database (GFED) products (VanderWerf2010) and the Fire INventory from NCAR (FINN) (Wiedinmyer2011), for instance, use this approach. GFED was developed for understanding monthly contribution of fires to global carbon cycling (VanderWerf2004), while FINN was developed for near real-time estimation (Wiedinmyer2011). The second technique deduces fuel consumption from Fire Radiative Power (FRP) determined from infrared thermal measurements. Two emission inventories use this approach, the Global Fire Assimilation System (GFAS) (Kaiser2012) and the Quick Fire Emissions Database (QFED) (Darmenov2015). Several studies used and compared these fire emissions inventories and found several differences in capturing wildfire activity over different areas as well as sources of uncertainties from the cloud gap adjustments, small fires estimations and land use and land cover estimation

(Liu2020). While these fire emission inventories all use the MODIS thermal anomalies (Giglio2006), they use different methods of translating emission factors and land cover to estimate fire emissions. Although the quantification of emissions from biomass burning from space-based instruments has increased significantly, uncertainties regarding input data and methodologies can still lead to errors up to an order of magnitude for the total trace gases emissions (Vermote2009, Baldassarre2015).

Moving from global annual fluxes to finer scales in space and time complicates the inference a great deal. Interpreting atmospheric measurements of CO_2 at these scales requires the use of an atmospheric chemistry transport model (CTM) and optimal estimation machinery assimilation system, frequently referred to in the literature as "atmospheric inversions", or "top-down inversions". However, even using the same set of observations such as the Orbiting Carbon Observatory 2 (OCO-2) data in different inverse modeling systems can induced induce a large range of CO_2 fluxes estimation at regional scales (Crowell2019,Peiro2022). Flux estimates from top-down inversions have been shown to be sensitive to the choice of transport model (Schuh2019), and observational coverage (Byrne2017). Even more importantly, atmospheric measurements of CO_2 dry air mole fractions represent the combined influence of all upstream emissions and transport, and so individual tracer measurements cannot be used to differentiate between different source or sink processes without more information. Additionally, prior estimate of the fluxes and their associated uncertainties can impact posterior CO_2 estimations (Lauvaux2012a, Lauvaux2012, Byrne2017,Gurney2003,Wang2018,Chevallier2005,Baker2006,Baker2010). A few studies (Liu2017, Palmer2019, Crowell2019, Peiro2022) utilized XCO_2 from OCO-2 to constrain top-down surface fluxes of CO_2. All of the mentioned studies found the Tropics to be a large source region for 2015-2016, though the explanations varied. Crowell2019 showed that an ensemble of inversion models delivered robust results for Tropical regions when OCO-2 data was assimilated. The ensemble employed included different atmospheric transport models, prior ocean and terrestrial biosphere and fire fluxes, and assimilation techniques. All of the participating models did not optimize fire and fossil fuel emissions. As such, only the non-fossil land (net biosphere exchange; NBE) and ocean flux at regional scales was examined in the study, with no attempt to attribute ensemble spread to different sources of uncertainty, such as the assumed fire emissions, which neglected to include some of the global inventories, such as FINN, QFED, and GFED4.1s (earlier versions of GFED were included).

Most inversion models do not explicitly constrain fire emissions with CO_2 observations. Rather, it is assumed that fire emissions have much lower uncertainty (generally believed to be less than 10% (LeQuere2018,Quilcaille2018)) than the ocean and terrestrial biosphere fluxes (LeQuere2018,Khatiwala2009,Khatiwala2013), and so are held fixed, with the net ecosystem exchange (NEE) being assumed to be the residual between the posterior total net land flux and the assumed fire and fossil fuel emissions. This inference is problematic, not least due to the aforementioned fire emissions uncertainties in time and space, which could alias into inferred biospheric fluxes at continental or regional scales (WiedinmyerNeff2007,Peylin2013). To reduce the uncertainties associated with fires and consequently with CO_2 biospheric emissions, we can examine gas species that are co-emitted with CO_2 from fires, such as carbon monoxide (CO).

CO is an air pollutant that affects the oxidation capacity of the atmosphere through its reaction with the hydroxyl radical (OH), leading to a relatively short atmospheric lifetime of one to three months because of its fast oxidation with OH. Reactions between CO and OH impact atmospheric composition on hemispheric (mainly in the Tropics) or even global scales (Logan1981). CO also leads to the formation of tropospheric ozone (O_3), an important short-lived greenhouse gas, and CO_2.

CO is produced by incomplete combustion, i.e. when there is not enough oxygen to make CO_2 (VanderWerf2010), such as in the case of smoldering fires. In this way, CO_2 is strongly co-emitted with CO in the presence of combustion (Bakwin1997, Potosnak1999, Turnbull2006). Previous studies used trace gases such as CO to improve the CO_2 flux estimation or to separate CO_2 emissions sources. Wang2010 used the CO_2/CO correlation slope to differentiate the source signature of CO_2 and separate the different characteristics of CO_2 emissions between rural and urban sites in China. Basu2014 estimated CO_2 emissions with Greenhouse gases Observing SATellite (GOSAT) data and the Comprehensive Observation Network for TRace gases by AIrLiner (CONTRAIL) project and studied seasonal variations of CO_2 fluxes during the 2009 and 2011 period over Tropical Asia. By using the Infrared Atmospheric Sounding Interferometer (IASI) CO measurements, their study showed an increased source of CO_2 in 2010 that was caused not by rising of biomass burning emissions but by biosphere response to above-average temperatures. In addition to CO, some studies worked on the correlation between additional species and CO_2 to constrain CO_2 emission from biomass burning. Konovalov2014 used satellite CO and aerosol optical depth data to constrain CO_2 emissions from wildfires in Siberia by estimating FRP to biomass burning rate conversion factors. Using this approach, they found that global emissions inventories underestimated CO_2 emissions from Siberia from 2007 to 2011.

As biomass burning emissions estimates are necessary for constraining top-down CO_2 emissions, we want to provide our CO_2 inversion model with fire emissions that contain as much realism as possible. Fires that incorporate information from both traditional bottom-up estimation techniques and atmospheric CO data may provide a better estimate than the global inventories alone. The corresponding top-down CO_2 fluxes imposing these optimized fire emissions should have more fidelity, particularly in the Tropics, where fires and the biosphere strongly interact with one another, and especially during severe drought conditions associated with the 2015 El Niño. The objective of this paper is to assess the improvement in CO_2 biogenic emissions estimates when CO-informed fire emissions are imposed, particularly during the 2015 El Niño event and the post-event subsequent years (2017 and 2018). First, we constrain CO emissions using data from the Measurements of Pollution in The Troposphere (MOPITT). We use these optimized CO emissions together with key vegetation parameters from GFED to create an updated estimate of fire CO_2 emissions that incorporates both sets of information. Finally, these updated fire emissions are imposed in an atmospheric CO_2 inversion that constrains CO_2 fluxes, using either OCO-2 XCO_2 retrievals or in situ data, with different assumed fire emissions and appropriately rebalanced prior biogenic fluxes.

This paper is ordered as follows. The assimilation and evaluation data sets and the inversion modeling framework are described in Section 2. The results for CO and CO_2 flux estimates and evaluation against independent data are presented in Section 3. The importance of these inversion results for conclusions about the terrestrial biosphere using top-down inversion models is are discussed in Section 4. Conclusions and proposed future work are presented in Section 5.

2 Data and methodology

Our experiments focus on estimation of top-down fluxes using the TM5-4DVAR system (e.g. Meirink2008, Basu2013, Crowell2018). Our inversions are performed in sequence, first assimilating total column CO retrievals from the MOPITT v8 products to produce optimized CO fluxes which are used to update the assumed CO_2 fire emissions, and then we optimized CO_2 fluxes

using total column CO_2 from OCO-2 version 9 retrievals or in situ data. Our inversions are performed in sequence: (1) we assimilate total column CO retrievals from the MOPITT v8 products to produce optimized CO fluxes, which are used to update the assumed CO2 fire emissions, and then (2) we assimilate either total column CO2 from OCO-2 version 9 retrievals or CO2 in situ data to produce optimized CO2 NEE and ocean fluxes. We introduce hereafter the observations used in the inversions, the inversion system and the observations used for validation.

2.1 Data sets

2.1.1 MOPITT data

Space-based CO data are available from a large variety of instruments: IASI (Infrared Atmospheric Sounding Interferometer, Turquety2004, Clerbaux2009) on-board Metop satellite, MOPITT (Measurements of Pollution in the Troposphere, Drummond2010, Drummond2016) on-board the Terra satellite, the Tropospheric Emission Spectrometer (TES, Beer1999) on-board EOS-Aura and the Atmospheric InfraRed Sounder (AIRS, Aumann2003) on-board EOS-Aqua. These satellite data can be used to monitor fire emissions from an atmospheric point of view. So far, MOPITT has been the only space-based instrument deriving CO from near-infrared (NIR), thermal infrared (TIR) and multispectral radiances (TIR + NIR). Recently, TROPOspheric Monitoring Instrument (TROPOMI, Landgraf2016) and GOSAT-2 TANSO-FTS-2 (http://www.gosat-2.nies.go.jp/) are also retrieving CO from NIR radiances. However, MOPITT products have been consistently validated against airborne vertical profiles and ground based measurements, allowing a well-understood of its continuity and consistency providing a well-understood product (Worden2010, Deeter2019).

MOPITT (Drummond1993) was launched in 1999 on board the Terra satellite. Terra flies in a sun-synchronous polar orbit at an altitude of 705 km, crossing the equator at approximately 10:30 local time each morning and evening. It has a nadir view with spatial resolution of 22 x 22 km. Its swath is 650 km wide, with 116 cross-track footprints. MOPITT achieves a global coverage in about 4 days.

MOPITT uses gas filter correlation radiometry to retrieve CO mixing ratios from radiances in the 4.7 μm (TIR) and 2.3 μm (NIR) spectral bands. TIR-only retrievals of MOPITT have been shown to be mostly sensitive to CO in the mid-upper troposphere (excluding regions with strong thermal gradients such as deserts, (Deeter2007)). NIR-only retrievals depend on reflected solar radiation, and are also used for retrievals of CO total column, though the vertical sensitivity is stronger near the surface than the TIR-only retrievals (Deeter2009, Worden2010). MOPITT TIR + NIR retrievals can provide improved estimates of CO near source locations and has enhanced land surface sensitivity compared to the TIR only product (Deeter2015). In this study, we consequently use the level 2 TIR-NIR profiles product in order to have better sensitivity of CO on the total column with greatest sensitivity in the lower troposphere (Deeter2013). With the observing limitations of NIR data, this product is limited to daytime observations over land. In addition, because retrievals with surface pressures less than 900 hPa might be of lower quality, they are removed for the assimilation (Fortems-Cheiney2011, Yin2015). MOPITT retrieval products are generated with an optimal estimation-based retrieval algorithm and a fast radiative transfer model involving both MOPITT calibrated radiances and a priori knowledge of CO variability (Deeter2003). The MOPITT operational fast forward model (MOPFAS) is a radia-

tive transfer model based on HITRAN2012 (Rothman2013) database with CO parameters in log(VMR) used to simulate the MOPITT measured radiances (Edwards1999). For this retrieval method, cloud-free observations are required. The MOPITT v8 products consist of CO profile with 10 pressure levels. In our assimilation system, simulated values of log XCO using the MOPITT v8 averaging kernel are compared to the retrievals, and the difference is then propagated into flux adjustments using the TM5 adjoint.

Several studies have used inverse modelling with MOPITT data to estimate CO emissions (Huijnen2016, Yin2016, Nechita-Banda2018) and they showed that MOPITT v7 data have poor performance at detecting extreme events. However, MOPITT v8 implemented a bias correction in the radiance which demonstrated improved retrievals relative to v7 (Deeter2019). In particular, MOPITT v8 does not exhibit a latitudinal dependence in partial CO column biases observed in v7 (Deeter2019). MOPITT v8 TIR-NIR product biases are within 5% at all levels when compared to NOAA aircraft profiles. In addition, apparent long-term trends in v7 biases have been decreased to 0.1%/yr or less at all retrievals levels for v8 products (Deeter2019). We thus expect to have better performance in the detection of extreme events by assimilating MOPITT v8 and less bias in the inferred CO emissions overall.

2.1.2 OCO-2 data

The OCO-2 (Crisp2017,Eldering2017) satellite was launched in July 2014 as the first NASA mission dedicated to observing CO_2 from space. The satellite flies in a sun-synchronous orbit with an altitude of 705 km and a 16 day revisit time. OCO-2 passes each location at approximately 13:30 local time (Crisp2004). OCO-2 observes 8 footprints across a 10 km ground track, each of which is less than 1.29 km by 2.25 km (Eldering2017). Smaller spatial footprints increase the number of cloud-free scenes allowing for more successful retrievals with lower errors (ODell2018), e.g. relative to the Greenhouse Gases Observing Satellite (GOSAT; Kuze2009).

OCO-2 measures the absorption of solar reflectance spectra within CO_2 (1.6 μm and 2.0 μm) and molecular oxygen (O_2) bands (0.76 μm). Retrievals from OCO-2 have sensitivity throughout the entire troposphere with highest sensitivity close to the surface (Eldering2017). As with CO, retrievals of CO_2 from TIR observations such as those from TES or AIRS typically have lower sensitivity in the atmospheric boundary layer (Eldering2017).

CO_2 retrieval products come from the Atmospheric Carbon Observations from Space (ACOS) retrieval algorithm (ODell2012, Crisp2012, ODell2018, Kiel2019). OCO-2 radiance measurements are analyzed with remote sensing retrieval algorithms to spatially estimate column-averaged CO_2 dry air mole fraction, XCO_2. This quantity represents the average concentration of CO_2 in a column of dry air from the surface to the top of the atmosphere. ACOS XCO_2 product have been largely validated against ground-based observations from the Total Column Carbon Observing Network (TCCON; (Wunch2017)). Our study uses the OCO-2 version 9 data product, as it contains all of the improvements as well as a bug fix that was found after the release of the version 8 (v8). Being a nonlinear optimal estimation product, retrievals contain residual errors that must be removed through the use of a bias correction (ODell2018, Kiel2019). Residual biases in XCO_2 were reduced especially over rough topography, which were found to be caused by relative pointing offsets between the three bands. Even after the bias correction is applied, errors on regional scales likely remain (ODell2018). Despite these shortcomings, data coverage from

satellites is dense in the Tropics relative to the global in situ network, which has very few sites there. Despite biases with satellite data but thanks to their large spatial coverage, several studies prefer to use satellite data over the Tropics. Despite the known shortcomings (biases) of satellite data, several studies have preferred to use satellite data over the Tropics to take full advantage of the improved spatial coverage. For instance, Liu2017 and Palmer2019 have discussed the impacts of the 2015-2016 El Niño event on the carbon cycle, particularly in the Tropics using OCO-2 v7. In addition, OCO-2 retrievals have been used in several inversion models. For example, (Crowell2019) showed that with different assumptions (such as a large ensemble of atmospheric inversions using different CTM, data assimilation algorithms, and prior flux), OCO-2 posterior inferred fluxes globally agree with in-situ data, but that this agreement breaks down quickly at redsmaller space and time scales. smaller spatial and temporal scales.

To finish regarding the data we are using in our study, (Huijnen2016) and (Patra2017) have shown that pyrogenic CO_2 emissions estimates from CO MOPITT data (through the use of emission factors) are consistent with OCO-2 measurements using a forward simulation with a CTM. With this in mind, and also that OCO-2 and MOPITT have similar vertical sensitivity for their retrievals of CO_2 and CO, we use these two data sets to constrain surface fluxes for these two tracers. Using CO_2 and CO together in this way is an important proof of concept for upcoming missions such as GeoCarb (Moore2018), which will measure both tracers from geostationary orbit over the Americas.

2.1.3 In situ data

The in situ CO_2 data used for assimilation come from 5 collections in ObsPack format (Masarie2014). These collections include :

- the obspack_co2_1_GLOBALVIEWplus_v5.0_2019-08-12 (obspack-gvp5.0) which contribute to 93% of all data.

- obspack_co2_1_NRT_v5.0_2019-08-13 (obspack-nrt5.0) which provides near-real time provisional observation and so the data did not get final quality control.

-obspack_co2_1_AirCore_v2.0_2018-11-13 which is provided by the balloon-borne AirCore instrument. This dataset includes almost the entire atmospheric column.

-obspack_co2_1_INPE_RESTRICTED_v2.0_2018-11-13 (obspack-INPEv2.0). This collection of data only comes from aircraft profiles at fives sites in Brazil.

-obspack_co2_1_NIES_Shipboard_v2.1_2019-06-12. The data come from 9 volunteer ships of opportunity operated by the Japanese National Institute for Environmental Studies (tohjima05a, nara17a).

These 5 collections provide around 540 assimilable observations per day. These CO_2 measurements are collected in flasks or by continuous analyzers at surface, tower, and aircraft sites (see Fig.) and are an important anchor for this exercise because their error characteristics are generally well-known, being directly established via calibration traceable to World Meteorological Organization standards. Additionally, these measurements provide traceability to a long history of flux estimates derived from these data as an atmospheric constraint.

2.1.4 Observations for validation : TCCON data

We evaluate our posterior model mole fractions against retrievals from TCCON, which is a ground-based network of Fourier transform spectrometers established in 2004 and designed to retrieve atmospheric gases from NIR spectra (Wunch2011). The global monthly means of the total column CO_2 measurements have accuracy and precision better than 0.25% (less than 1 ppm) relative to validation with aircraft measurements (Wunch2010, Wunch2011). TCCON measurements have been used in several papers for validation of satellite measurements (e.g. (Kulawik2016,Wunch2017,ODell2018,Kiel2019)). Our evaluation uses data from 23 operational instruments of TCCON globally. Table 1 lists all TCCON sites used for the evaluation and Fig. S1bb represents the location of the sites over the globe.shows the site locations over the globe.

Table 1. Geolocation and reference of each TCCON station used for the evaluation section.

TCCON sites	Country	Latitude	Longitude	Data revision	Reference
Eureka	Canada	80.05N	86.42W	R3	https://doi.org/10.14291/tccon.ggg2014.eureka01.r3
Ny-Ålesund	Spitsbergen	78.9N	11.9E	R0	https://doi.org/10.14291/tccon.ggg2014.nyalesund01.r0/1149278
Sodankylä	Finland	67.4N	26.6E	R0	ggg2014.sodankyla01.R0
Białystok	Poland	53.2N	23.0E	R2	https://doi.org/10.14291/tccon.ggg2014.bialystok01.r2
Bremen	Germany	53.10N	8.85E	R0	ggg2014.bremen01.R0
Karlsruhe	Germany	49.1N	8.4E	R1	https://doi.org/10.14291/tccon.ggg2014.karlsruhe01.r1/1182416
Paris	France	48.8N	2.4E	R0	https://doi.org/10.14291/tccon.ggg2014.paris01.r0/1149279
Orléans	France	47.9N	2.1E	R1	https://doi.org/10.14291/tccon.ggg2014.orleans01.r1
Garmisch	Germany	47.5N	11.1E	R2	https://doi.org/10.14291/tccon.ggg2014.garmisch01.r2
Park Falls	Wisconsin (USA)	45.9N	90.3W	R1	https://doi.org/10.14291/tccon.ggg2014.parkfalls01.r1
Rikubetsu	Japan	43.5N	143.8E	R2	https://doi.org/10.14291/tccon.ggg2014.rikubetsu01.r2
Lamont	Oklahoma (USA)	36.6N	97.5W	R1	ggg2014.lamont01.R1
Anmeyondo	Korea	36.5N	126.3E	R0	ggg2014.anmeyondo01.R0
Tsukuba	Japan	36.1N	140.1E	R2	https://doi.org/10.14291/tccon.ggg2014.tsukuba02.r2
Edwards	California (USA)	34.2N	118.2W	R1	ggg2014.edwards01.R1
Caltech	California (USA)	34.1N	118.1W	R0	ggg2014.pasadena01.R1
Saga	Japan	33.2N	130.3E	R0	ggg2014.saga01.R0
Izaña	Tenerife	28.3N	16.5W	R1	https://doi.org/10.14291/tccon.ggg2014.izana01.r1
Ascension Island	UK	7.9S	14.3W	R0	ggg2014.ascension01.R0
Darwin	Australia	12.4S	130.9E	R0	ggg2014.darwin01.R0
Réunion Island	France	20.9S	55.5E	R1	https://doi.org/10.14291/tccon.ggg2014.reunion01.r1
Wollongong	Australia	34.4S	150.9E	R0	ggg2014.wollongong01.R0
Lauder 125HR	New Zealand	45.0S	169.7E	R0	ggg2014.lauder01.R0

2.2 Chemistry transport model TM5

We employ TM5 (Krol2005) and the Four-dimensional Variational (4DVAR, Meirink2008) framework to link trace gas emissions to atmospheric tracer mixing ratios. Several inverse modelling studies have estimated CO emissions or CO_2 emissions using TM5-4DVAR (Hooghiemstra2011,VanLeeuwen2013,VanderLaan-Luijkx2015, Nechita-banda2018, Basu2018, Crowell2018,Crowell2019). TM5 is driven by 3-hourly offline meteorological fields from the ERA-Interim (Dee2011) reanalysis of the European Centre for Medium range Weather Forecasts (ECMWF). We run TM5 on a 3°x2° horizontal resolution grid for the CO inversion and on a 6°x4° horizontal resolution grid for the CO_2 inversions with 25 vertical hybrid sigma-pressure levels. The initial condition for CO is globally constant to 80ppb, which is then combined with a 6 month spin-up to account for discrepancies from the real atmospheric distribution of CO. The initial global distribution of CO_2 is taken from the CarbonTracker ((Peters2007) version CT2017, with updates documented at http://carbontracker.noaa.gov) posterior mole fractions. The CT2017 fields are constrained over the period 2000-2016 with data from the global in situ network. Both inversions are run from July 1, 2014 until March 1, 2019, i.e. with six months of spinup and two months of spindown to avoid so-called "edge effects" affecting the period of interest from 2015-2018.

The CO sink from OH is represented in TM5 by a monthly OH climatology from Spivakovsky et al., (2000). This OH climatology is scaled by a factor 0.92 based on methyl chloroform simulations (Huijnen et al., 2010).

2.3 Inversion system and analyses

We use TM5-4DVAR to infer fluxes as the long window ensures a long term spatio-temporal distribution of the trace gas in the atmosphere that is consistent with multi-year flux distributions. The TM5-4DVAR model is used in this study to estimate CO and CO_2 emissions with the corresponding satellite and in situ data. TM5-4DVAR utilizes optimal estimation to minimize a Bayesian cost function (Rodgers2000) in order to find the state vector corresponding to surface emissions of CO or CO_2 that best match the observations within their relative uncertainties. The a posteriori flux is found by minimizing the mismatch between the forward model and the observations weighted by the inverse of the observation error covariance matrix **R** while staying close to a set of a prior fluxes weighted by the inverse of the a priori error covariance matrix **B**. These matrices are discussed in more detail in Section 2.3.1. Although the CTM is quasi-linear, the observation operator for CO is not. Since we use log(VMR) for the MOPITT retrievals as the CO observable, the non-linear optimizer M1QN3 from (GilbertLemarechal1989) is employed. Both the transport and observation operators for CO_2 are linear, and so we employ the conjugate gradient method to estimate the optimal CO_2 emissions, the implementation of which is described in great detail in (Basu2013).

2.3.1 A priori information

a) CO parameterizations

Injection heights, in the CO inversion, are computed using IS4FIRES (Integrated System for Wild-Land Fires, http://is4fires.fmi.fi/, Sofiev2013). This emission database is driven by re-analysis FRP obtained from MODIS (Giglio2006)) instrument on board Aqua and Terra satellites.

Three emissions categories are used for the CO inversion : anthropogenic (which represents the combustion of fossil fuels and biofuels), natural sources (direct CO emissions from vegetation and oceans) and biomass burning (vegetation fires). In our configuration, we only optimize biomass burning emissions.

Anthropogenic emissions come from MACCity inventory (Granier2011). This inventory provides projected inter-annual trends in the anthropogenic CO emissions.

The oxidation of CH_4 and non-methane volatile organic compounds (NMVOCs) such as isoprene (C_5H_8) and monoterpene ($C_{10}H_{16}$) leads through photolysis and reaction with OH to the formation of formaldehyde, the major chemical source of CO (Atkinson2000). Isoprene is a member of the group of hydrocarbons known as terpenes. It is explicitly taken into account in TM5 as it represents the dominant biogenic NMVOC emission (Guenther2012). Isoprene and monoterpene oxidation schemes are based on the mechanisms developed by (Yarwood2005). Isoprene contributes to 9-16 % of the global CO burden (Pfister2008). They account for 68% in TM5 of the biogenic NMVOC emissions that react to produce CO. By contrast, monoterpene accounts for 15% (Tsigaridis2014). The chemical production of CO coming from the oxidation of methane and NMVOCs requires monthly 3-D CO fields produced by oxidation of biogenic and anthropogenic hydrocarbons including CH_4. We use chemical production of CO from the oxidation of CH_4 and from NMVOCs by using a 2010 simulation with the full chemistry version of TM5 (Huijnen2010).

A priori biomass burning CO emissions are taken from the GFED4.1s inventory (VanderWerf2010) and incorporate a daily cycle.

The first version of GFED was released in 2004. Since then, several improvements have been incorporated into GFED. Improvement on the mapping of burned area from active fire data in GFED2 (Giglio2006) was no longer necessary when the MODIS product became available for GFED3 (Giglio2010). Burned area particularly affects the spatiotemporal variability of carbon emissions during fires. This spatiotemporal impact has been implemented in GFED with biogeochemical modeling framework providing estimation of biomass combustion over different vegetation types (Giglio2013). All GFED versions are then based on the Carnegie-Ames-Standford Approach (CASA) model adjusted to account for fires (see VanderWerf2004 and VanderWerf2017 for more details). The most recent versions (GFED4 and GFED4.1s which includes small fire burned area) modified the burned-area-to-burned fraction conversion, which have been shown to increase burned area and fire carbon emissions of 11% in GFED4.1s compared to GFED3 (VanderWerf2017) at the global scale. JCLiu2017 found that with the omission of small fires in GFED3, global fire emissions are underestimated. Accounting for small fires increased global burned area and carbon emissions by 35% (Randerson2012), and improved the agreement of spatial distribution between active fires and burned area over regions with large fires such as savanna fires and boreal forests. Including small fires in GFED amplifies emissions over regions where drought stress and burned area varied considerably from year to year in response to, for instance, the El Niño Southern Oscillation (ENSO). the GFED4.1s burned area are based on fire observations from the MODIS instrument with a 500 m horizontal resolution. The MODIS burned area data have been combined with active fire data from Tropical Rain-

fall Measuring Mission (TRMM), the Visible and Infrared Scanner (VIS), and the Along-Track Scanning Radiometer (ATSR), three other instruments on board with MODIS. GFED4.1s has a spatial resolution of 0.25°x0.25° and includes estimates of burned area, carbon emissions, monthly biospheric carbon fluxes based on the CASA-GFED4s framework and the information from small fire fraction. Additionally, monthly carbon emissions of GFED4.1s distinguish between different vegetation types such as boreal forest, agricultural waste, temperate forest, deforestation, peat-land, and savanna.

The prior uncertainty covariance matrix **B** is described by a product of uncertainty variance and correlations in space and time. Spatially, a Gaussian correlation length scale of 1000 km is used ,as justified in Meirink et al., (2008), while we assume the prior errors have a temporal correlation scale of 4 days. As in Hooghiemstra2011, Hooghiemstra2012 and NechitaBanda2018, an uncertainty standard deviation of 250% has been applied for the grid-scale prior of biomass burning emission. This large uncertainty is assumed since these inventories support large uncertainties. As mentioned by Hooghiemstra2011, this yields between 40-100% of prior continental emissions uncertainty, depending on the region. The errors are assumed uncorrelated leading to a diagonal observational error covariance matrix **R**.

b) Computation of an optimized CO_2 Fire Prior

In this section, we describe the computation of our optimized prior fire emission blue(FIREMo) which we will use to observe the impact of CO fire emissions in the posterior CO_2 biospheric fluxes. The flowchart of FIREMO calculation steps is shown in Fig. 1. For each pixel of CO posterior biomass burning fire emissions constrained by MOPITT retrievals, we break down the global CO fire emissions using the GFED4.1s partitioning in order to obtain posterior simulated CO fire emissions applied a vegetation fraction based on the dry matter product (DM) of GFED4.1s. We obtained fire emissions for each monthly vegetation type for each monthly vegetation type (savanna, boreal forests, peat, temperate forests, deforestation and agriculture waste). Figure 3 S1 shows for instance the GFED DM vegetation type for each year over land , where each pixel represents one or more vegetation types.. Each color represents pixel with one or several vegetation types.

We first calculated the emission ratios $ER_{(CO/CO_2)}$ which allowed us to convert CO fire emissions to CO_2 fire emissions. The emission ratios are computed using the GFED emission factor for each vegetation type (annotated *i* in the equation 1). Following the equation of AndreaeMerlet2001 :

$$ER_{(CO/CO_2)_i} = \frac{EF_{CO\,i}}{EF_{CO_2\,i}} . \frac{M_{CO_2}}{M_{CO}} \tag{1}$$

with $M_{CO} = 28$ g.mol^{-1} and $M_{CO_2} = 44$ g.mol^{-1} the molecular weights of CO and CO_2; EF are the emission factors for each vegetation types describes in table 2. Emission factors allow us to estimate trace gases emissions from carbon losses during fires (AndreaeMerlet2001). For better comparison and as the CMS-GFED3 product (we will introduce later) used the emission factor of Andreae and Merlet (2001) and Akagi et al., (2011), we applied the same emission factors and consequently did not use the new estimate established by Andreae et al., (2019).

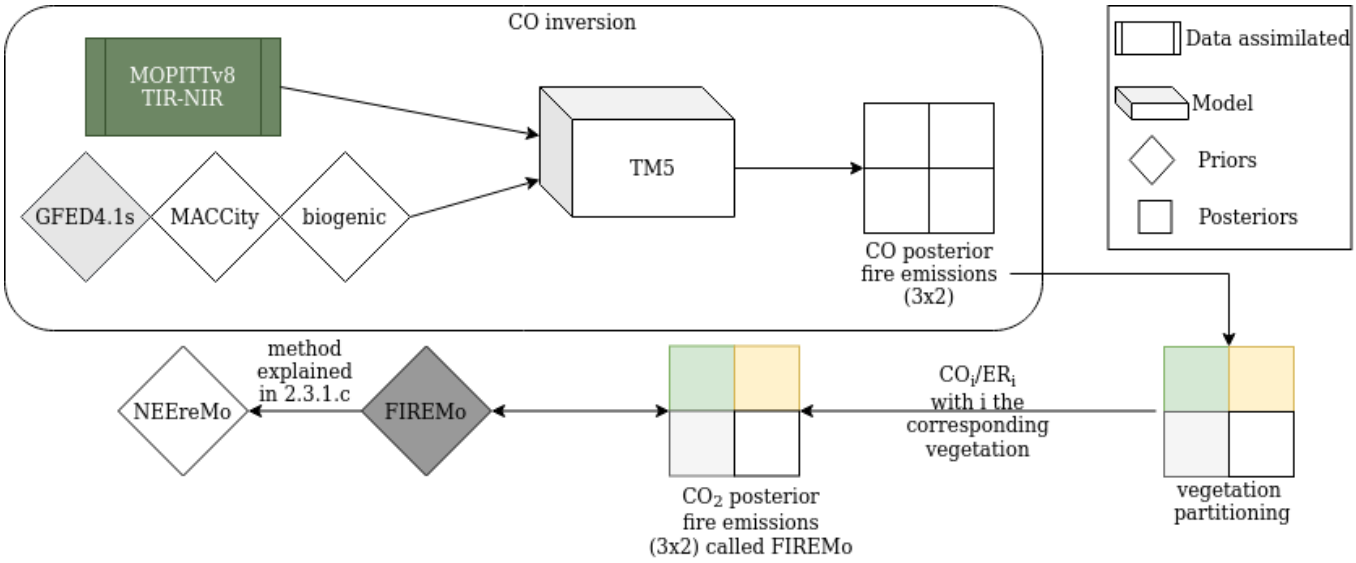

Figure 1. Flowchart of the FIREMO calculation from the CO inversion

Table 2. Emission Factors in $g.kg^{-1}.DM^{-1}$ for CO and CO_2, and emission ratios $ER_{(CO/CO_2)}$ available from GFED4.1s by vegetation types based on van der Werf et al., (2017).

	Savanna	Boreal forests	Temperate forests	Deforestation	Peat	Agriculture waste
EF_{CO}	63	127	88	93	210	102
EF_{CO_2}	1686	1489	1647	1643	1703	1585
$ER_{(CO/CO_2)}$	0.059	0.134	0.084	0.089	0.194	0.101

We then aggregated the 0.25°x0.25° vegetation fraction partitioning of GFED to create vegetation masks fraction product at a 3°x2° grid (see Fig. 1). We applied this aggregated mask fraction to the posterior simulated CO fires, which partitioned the posterior CO fires by vegetation types (we took care to divide the emissions by number of vegetation found by pixel). Finally, the emission ratio for each vegetation type was divided into the posterior CO fire partitioned as used in Christian2003 and Basu2014 for each vegetation type (Basu et al., 2014). This results in monthly CO_2 emission per vegetation type per grid box at a 3x2 resolution. Finally, we sum up these emissions across all surface types in order to get monthly total optimized prior CO_2 biomass burning emissions that we called "FIREMo" (see Fig. 1). We used this FIREMo as the a fire prior emissions in CO_2 inversions along with a re-balanced respiration and NEE in order to have the net fluxes (in balance with fire estimate), using the parameterization described in the following section 2.3.1.c.

c) CO_2 parameterizations

CO_2 emissions are separated into four categories: anthropogenic sources, ocean fluxes, terrestrial biosphere fluxes (meaning the sum of the photosynthesis and respiration) and fires.

The anthropogenic emissions are taken from the Open-source Data Inventory for Anthropogenic CO_2 2018 (ODIAC2018; OdaMaksyutov2011). A diurnal cycle is imposed by TIMES product with weekly scaling as suggested by Nassar2013. Fossil fuel emissions are not optimized in the CO_2 inversions, as is typical of global tracer transport inversions (e.g. (Peylin2013,Crowell2019)). Ocean fluxes are taken from the climatological fluxes described in Takahashi et al., (2009). They are assumed to have an uncertainty variance of 50%. Both biospheric and oceanic emissions are optimized in the CO_2 inversions. The uncertainties in the prior fluxes are derived from different climatological fluxes with exponential spatio-temporal correlation assumed. For the oceanic component, the horizontal correlation is 1000 km and the timescales is 3 weeks, while for the terrestrial component, length and timescale are 250km and 1 week. These uncertainties are applied similarly to all experiments.

Terrestrial biosphere fluxes and fire emissions are difficult to disentangle a priori from CO_2 data alone, and some inverse modeling studies (e.g. Crowell et al., (2019)) choose instead to report the net land fluxes. Likewise, some global land flux estimates such as GEOS-Carb CASA-GFED3 project (Ott2020) use fire estimates to revise the terrestrial biosphere flux estimates through modification of ecosystem respiration. We take a similar approach, starting with the gross primary production and respiration estimates from the CASA-GFED3 3-hourly $0.5^\circ \times 0.625^\circ$ (Ott et al., 2020). We then modify the net flux in concert with each fire emissions estimated as follows.

Net ecosystem exchange (NEE) in the GEOS-Carb CASA-GFED3 product is expressed as the sum of heterotrophic respiration (Rh) and gross ecosystem exchange (GEE) :

$$NEE3 = Rh3 + GEE3 \tag{2}$$

We modified the respiration from CASA-GFED3 (*Rh3* , respiration linked to FIRE3) to create respiration estimates for GFED4.1s (*Rh4* , respiration linked to FIRE4) and FIREMo (*RhMo*, respiration linked to FIREMo linked with the FIREMo we calculated previously) which balance with the updated CO_2 fire estimate so that estimated respiration increases (decreases) in the places where each fire estimate is smaller (larger) than FIRE3 (GFED3):

$$Rhx = Rh3 + max(FIRE3 - FIREx, 0) \tag{3}$$

where x is either “4" or “Mo". This equation means that the difference between FIRE3 and FIREx is cut off at 0 when the difference is negative. With this equation we only consider the positive difference (when we have lower FIREx emissions than FIRE3). The resulting net ecosystem exchange, i.e. NEE4 or NEEMo, is then computed using (2), with *GEE3* used for both NEE4 or NEEMo equations. We then apply a simple rebalancing scheme to match the yearly NOAA global mean growth rate (AGR_{NOAA}) for 2015-2018 (see table 3), since

$$\mathrm{AGR} = \overline{\mathrm{NEE}} + \overline{\mathrm{FIRE}} + \overline{\mathrm{FOSSIL}} + \overline{\mathrm{BIOFUEL}} + \overline{\mathrm{OCEAN}} \tag{4}$$

where $\overline{X}$ represents the global total annual flux for category X. We use ODIACv2018 (with 2018 repeated for 2019) to compute the global fossil fuel totals (values in the table 3), BIOFUEL from the CASA land biosphere model (VanderWerf2004), and a fixed annual value of -2.6 PgC/yr for the oceans for simplicity, and we use FIRE from each source described above.

Table 3. Global total fossil fuel emissions, fire from GFED3 and GFED4.1s, FIRE (fire+biofuel) and biofuel emissions and AGR from NOAA in PgC/yr.

	2015	2016	2017	2018
BIOFUEL	0.479	0.476	0.486	0.486
FOSSIL FUEL	9.89	9.91	10.07	10.28
GFED3	2.03	1.63	1.97	1.97
GFED4	2.09	1.73	1.69	1.64
FIRE3	2.51	2.11	2.46	2.46
FIRE4	2.57	2.21	2.18	2.13
FIREMo	1.82	1.47	1.58	1.56
NEECMS	-3.23	-3.09	-5.11	-4.82
NEEre3	-3.22	-3.08	-5.11	-4.82
NEEre4	-3.23	-3.15	-4.83	-4.49
NEEreMo	-2.50	-2.43	-4.24	-3.93
AGR_{NOAA}	6.3	6.06	4.54	5.05

Any mismatch between the AGR derived from our prior flux estimates (AGR_x) and AGR_{NOAA} is assumed to be due to an incorrect estimate of global NEE. We adjust NEE at each gridpoint with a simple scaling on global total respiration (i.e. Rhx) and GEE:

$$AGR_{NOAA} - AGR_x = (1+k)\overline{\text{Rhx}} + (1-k)\overline{\text{GEE}}. \quad (5)$$

where x is either 3, 4, or Mo, depending on whether we use FIRE3 (GFED3), FIRE4 (GFED4.1s), or FIREMo. This equation is easily solved for k using each annual global total, and the resulting corrections are applied to each 3-hourly gridded value of GEE and respiration for each choice of fire emissions. In this way, the a priori global CO_2 emissions are ensured to match the annual global growth rate as measured by NOAA regardless of the fire emissions assumed, as well as a spatial pattern and seasonality that aligns with bottom up models' GEE and Rh estimates as closely as possible.

Table 4. Experimental Configurations

	CMS-GFED3	GFED3re	GFED4re	MOre
ODIAC Fossil	X	X	X	X
FIRE3 (GFED3 Fires)	X	X		
FIRE4 (GFED4.1s Fires)			X	
FIREMo (MOPITT Fires)				X
Takahashi Ocean Flux	X	X	X	X
Annual Total Matches AGR_{NOAA}		X	X	X

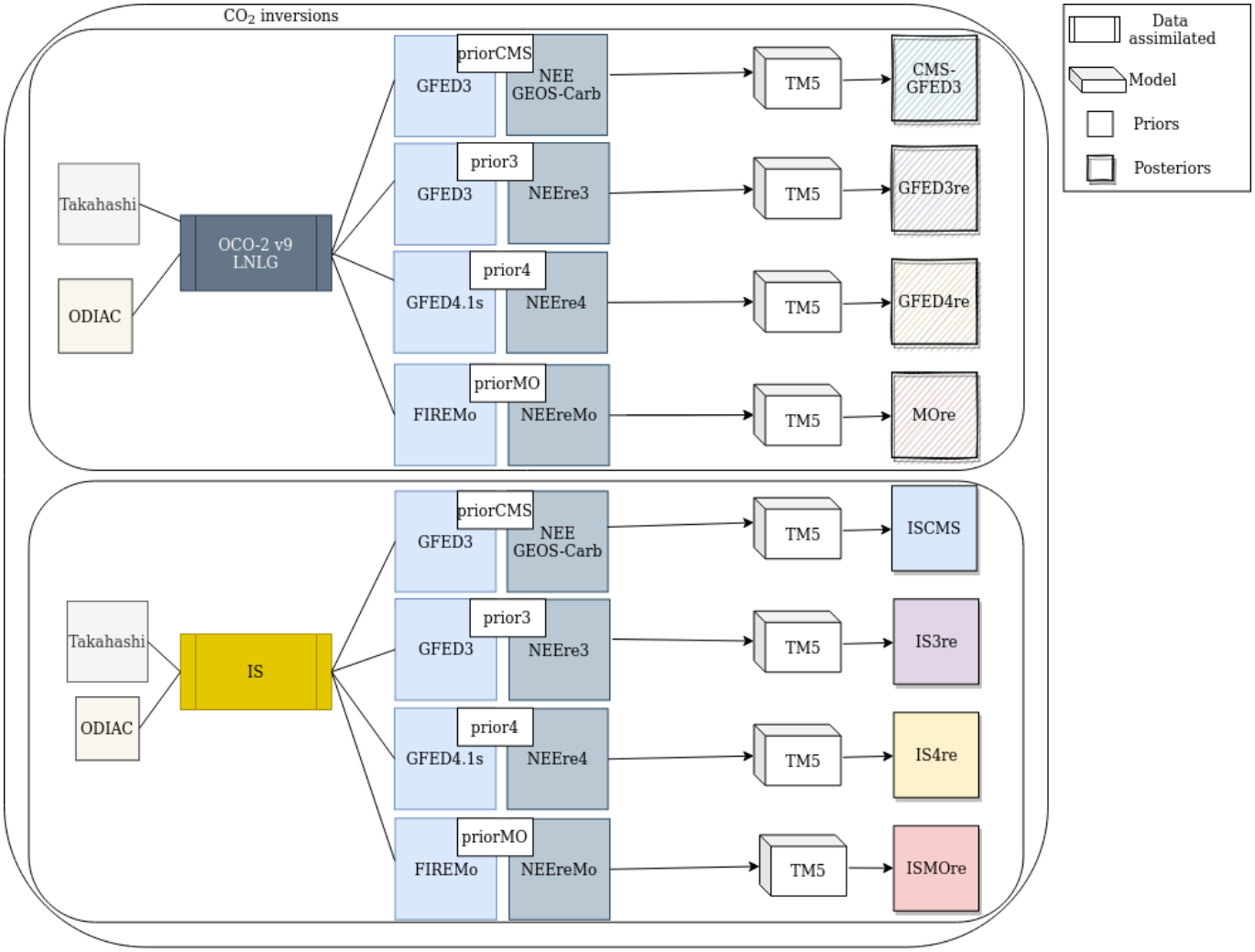

Figure 2. Flowchart of the six different CO_2 inversions performed.

We run the CO_2 inversions with the re-balanced terrestrial biosphere net flux NEEre*x* corresponding to either GFED3, GFED4 or FIREMo priors. In order to assess the impacts of the rebalancing procedure, we perform a fourth experiment that assumes the GEOS-Carb CASA-GFED3 NEE as the prior biosphere flux with GFED3 fires, and the results are labeled in what follows as CMS-GFED3. All CO_2 FIRE priors include both biomass and biofuel burning. The details of each of the 4 priors and the experimental configurations are detailed in table 4.

We optimized CO biomass burning emissions and CO_2 biospheric and oceanic emissions on a weekly basis. For the OCO-2 and in situ CO_2 inversions, we use four different sets of prior biosphere and fire emissions (see section 2.3.1).

3 Results

In section 3.1, we examine the impacts of assimilating MOPITT v8 XCO observations on inferred fire CO emissions after vegetation partition and the comparison with the prior GFED4.1s CO emissions categorized by vegetation type are the one used for developing FIREMo.

In section 3.2, we focus on the CO_2 inversions. As fire emissions are not optimized in CO_2 inversions, we will examine how posterior NEE varies according to observation constraint and the imposed fire fluxes. We first compare (in 3.2.1) the variability and magnitude between the biospheric priors used in the CO_2 inversions over the globe. zonal bands and over the same regions as in (Crowell2019), which are Transcom (Gurney2002) regions that are further subdivided at the equator (which we will called OCO-2 MIP regions). The regions are defined in Fig. 3 and are composed of 16 land regions and 11 ocean regions. We will focus on regions over land, as we are mostly interested in the interplay between assumed fire emissions and inferred NEE. We then investigate the covariation of imposed CO_2 fire emissions and optimized NEE with OCO-2 data and in-situ data (3.2.2). Finally, posterior simulated CO_2 mixing ratio are validated against TCCON data over the globe in section 3.2.3.

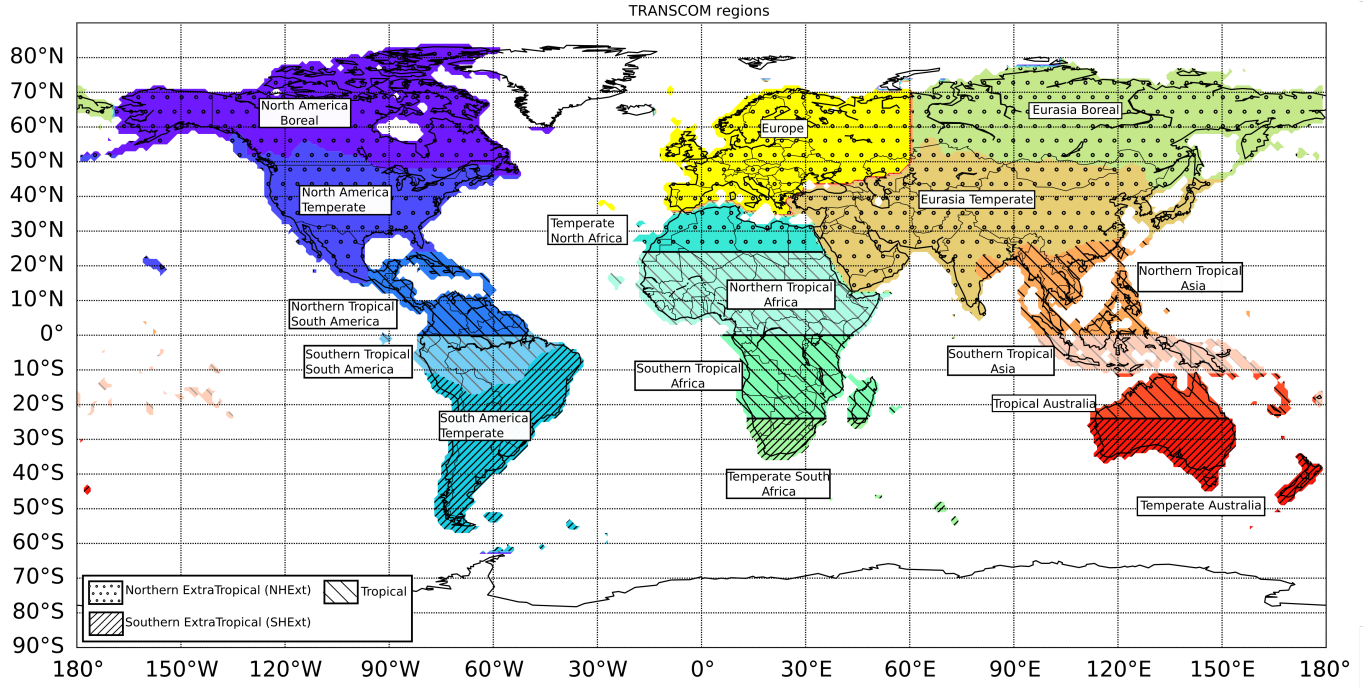

Figure 3. OCO-2 MIP regions for which prior and posteriors gridded fluxes are aggregated for comparison

3.1 Fire CO emissions partitioned by vegetation type : MOPITT optimized emissions versus GFED4.1s emissions

Figure 4 shows the annual CO fire emissions partitioned by vegetation combustion between MOPITT CO optimized fire emissions and fire prior (GFED4.1s) over the globe and by OCO-2 MIP regions. We can see globally, that depending on

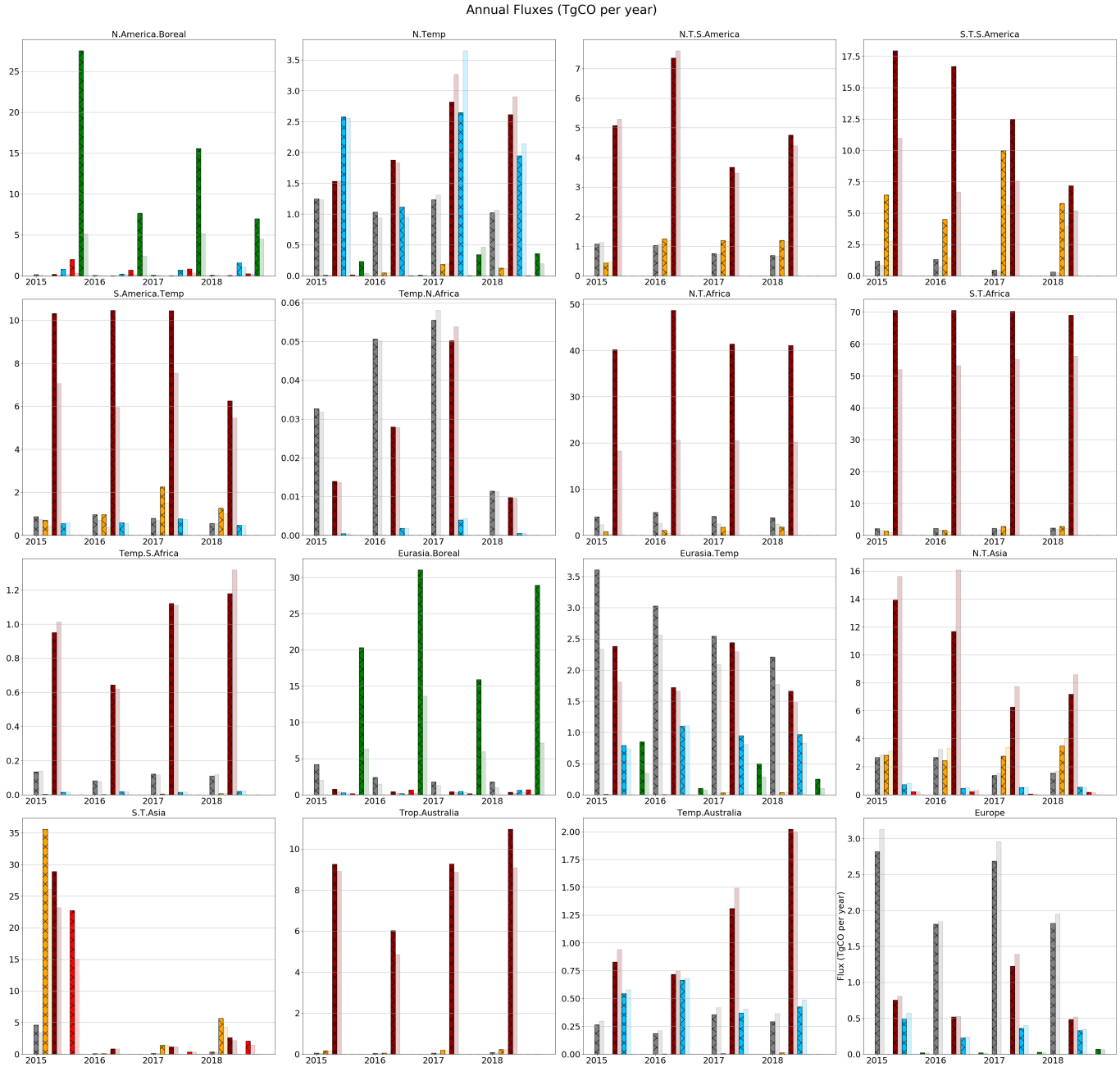

Figure 4. Annual CO fire emissions by vegetation type over the OCO-2 MIP regions between fire priors (hatch bars) and fire posterior from 2015 through 2018. Vegetation types are representing by colors : agriculture in gray, deforestation in yellow, savanna in dark-red, temperate forest in blue, peat land in red and boreal forests in green. Emissions are annually in TgCO/yr.

the regions, the assimilation of MOPITT data implies less or more CO fire emission than the prior. For instance, in 2015, the Northern Tropical South America shows more CO fire emissions for all types of vegetation (agricultural, savanna and deforestation) with the posterior while the Southern Tropical South America gives more CO with the prior for the same types of vegetation. For some other regions, such as Northern Temperate America and Temperate North Africa, MOPITT and GFED4.1s give almost the same amount of CO fire emissions for all types of vegetation. Over Temperate Northern Africa, this can be a result of bias satellite data due to cloud coverage, giving the CO posterior emissions closer to the prior GFED4.1s. However, for Northern Temperate America, the prior might be well enough constrained and validated over this region, to give similar CO fire emissions than the posterior CO. For Temperate North Africa, MOPITT posterior fires remain close to the prior GFED4.1s estimates, meaning that the inferred emissions are consistent with GFED4.1s. This region is known to have a lot of Saharan dust transported across the Atlantic ocean and towards Europe most of the year and to be largely cloudy during the wet season of the African monsoon (from May to August), which could explain the posterior emissions being close to the prior. This is also the case for Northern Tropical Africa, however, MOPITT posterior fires has lower emissions than the prior GFED4.1s estimate. But, we still need further investigation over Northern Tropical Africa to understand why GFED4.1s and MOPITT are different each other. Tropical South America is also known to have a cloudy coverage limiting satellite observations, but over this region we only observe similar emissions between the prior and the posterior for Northern Tropical America, even if MOPITT has slightly higher emissions, while for Southern Tropical America, differences between the prior and the posterior are strong. Differences between MOPITT posterior emissions and GFED4.1s are particularly large for Tropical Africa and for the boreal forests of North America and Eurasia with difference of more than 15 TgCO/yr. On average for the 2015-2018 period of study and for the regions Europe, North Tropical South America, Temperate South America, Temperate Australia and North Tropical Asia, MOPITT gives higher emissions for the deforestation types, savanna and agricultural waste. This is the case for the Northern Tropical Southern America and Australia, which are dominated by trees and grass savanna. This characteristic has been also observed by the previous study of Pechony2013 who compared the older version of GFED with MOPITT and TES emissions for the period 2005-2008. For Eurasia Temperate, discrepancies appear between MOPITT and GFED4.1s for all type of vegetation and for all years. These regions are characterized by agricultural waste and savanna, as well as temperate forests, regarding the GFED4.1s vegetation types. The discrepancies observed between MOPITT and GFED4.1s could then be that the vegetation type is not well represented for these regions. As mentioned in Pechony2013, agriculture and savanna vegetation types might not be the dominant burning vegetation type over North Africa and the Middle East, since these regions have seen an increase in croplands area well control by human activities and so burn rarely. However, Kazakhstan is a region of temperate forest often dominated by fires (Venevsky2019), a characteristic that MOPITT posterior emissions seem to observe as mush as the prior GFED4.1s. We can also observe that over Northern Tropical Asia, MOPITT fire emissions are higher than GFED4.1s (see Fig. 4 and Fig.**??**). This is observed for all years, where MOPITT emissions are almost 5 TgCO/yr (2 TgCO/yr) for savanna (for the other vegetation types) higher than from GFED4.1s. As mentioned in Petron2002 and Arellano2004, CO emissions in Northern Tropical Asia are significantly underestimated in current inventories. Previous studies have shown that peat area and depth, producing large amount of carbon ($\sim$ 0.60 PgC/yr which represents 26% of the total carbon fire emissions, NechitaBanda2018), were found to have significant uncertainties in Indonesia in the

emissions inventories (Lohberger2017, Hooijer2013). The added value of MOPITT CO observations is especially important for peat lands situated over Indonesia and Tropical Asia (see Fig. **??**). MOPITT tends to capture smaller fires due to the large field of view (Pechony2013). In addition, MOPITT can capture the seasonality of peat fires over Indonesia in comparison to GFED4.1s. Figure **??** shows for Southern Tropical Asia (mainly visible in 2015 due to the large emissions) that GFED4.1s have a fire peak earlier than MOPITT. VanderLaan-Luijkx2015 and Nechita-banda2018 hypothesized that GFED4.1s might not capture the timing of emissions over area with peat fires due to the use of burned area, which may be more sensitive to the initial stages of the fire than to the continued burning. Knowing this fact, and the large uncertainties attributed to fire emissions inventories in the Tropics, will be important for the following of this study in the computation of FIREMo and its uses in the CO_2 inversions. Overall, GFED4.1s gives higher CO fire emissions than MOPITT with some exception where MOPITT gives higher CO fire emissions particularly during the 2015-2016 El Nino period such as Northern Tropical South America and for agricultural waste, savanna and deforestation of Northern Tropical Asia.

Figure 4 shows the annual CO posterior and prior fire emissions split by vegetation combustion across the globe and by OCO-2 MIP regions. Overall, it can be seen that depending on the region, the assimilation of MOPITT data involves less or more CO emissions compared to the prior GFED4.1s. For North Temperate America, posterior emissions remain close to the prior estimates, suggesting that the inferred emissions are consistent with GFED4.1s. Comparable results are also observed for Temperate North Africa. However, this region is known to have a lot of Saharan dust transported across the Atlantic Ocean and towards Europe most of the year, which could explain the posterior emissions being close to the prior as those MOPITT soundings have largely been removed by pre-screeners. North Tropical Africa is not only affected by dust, but it is also largely affected by clouds during the wet season of the African monsoon (from May to August), which could lead to errors in retrievals that pass the pre-screeners. The combination of clouds and dust could explain the MOPITT posterior fires having lower emissions than the prior GFED4.1s estimate. But further investigation into North Tropical Africa is needed. Even though the prior is higher than the posterior for tropical Africa, in opposition to the previous multi-species study of Zheng et al., (2018), the posterior emissions better fit MOPITT measurement than the prior (Fig. S4). Tropical south America (including North Tropical South America and South Tropical South America) is also known to have cloud coverage limiting satellite observations. We however observe similar emissions between the prior and the posterior for the northern region, with slightly higher emissions for MOPITT. For the southern region, differences between the prior and the posterior are strong. The cloud coverage might explain this behavior, but further investigation are needed for these two regions. The discrepancies observed for Eurasia temperate between MOPITT and GFED4.1s could be that the vegetation type is not well represented for these regions. As mentioned in Pechony2013, agriculture and savanna vegetation types might not be the dominant burning vegetation type over North Africa and the Middle East, since these regions have seen an increase in croplands area well control by human activities and so burn rarely. However, Kazakhstan is a region of temperate forest often dominated by fires Venevsky2019, a characteristic that MOPITT posterior emissions seem to observe as mush as the prior GFED4.1s. We can also observe that over Northern Tropical Asia, MOPITT fire emissions are higher than GFED4.1s (see Fig. 4 and Fig.**??**). This is observed for all years, where MOPITT emissions are almost 5 TgCO/yr (2 TgCO/yr) for savanna (for the other vegetation types) higher than from GFED4.1s. As mentioned in Petron2002 and Arellano2004, CO emissions in Northern Tropical Asia

are significantly underestimated in current inventories. Previous studies have shown that peat area and depth, producing large amount of carbon (0.60 PgC/yr which represents 26% of the total carbon fire emissions, NechitaBanda2018), were found to have significant uncertainties in Indonesia in the emissions inventories Lohberger2017, Hooijer2013. Our posterior have lower emissions than the prior for southern tropical Asia, in contradiction to what Nechita-banda2018 observed. However, Nechita-banda2018 assimilated MOPITT and NOAA observations and used GFAS as fire priors, an inversions set-up different to what we used. Additionally, no evaluation against independent data have been performed in their study to determine if their results are more trustworthy than our results. Moreover, our posterior can capture the seasonality of peat fires over Indonesia in comparison to GFED4.1s. Figure **??** shows for Southern Tropical Asia (mainly visible in 2015 due to the large emissions) that GFED4.1s have a fire peak earlier than MOPITT. VanderLaan-Luijkx2015 and Nechita-banda2018 hypothesized that GFED4.1s might not capture the timing of emissions over area with peat fires due to the use of burned area, which may be more sensitive to the initial stages of the fire than to the continued burning.

3.2 OCO-2 and in situ CO_2 inversions with different fire and NEE priors

We performed inversions with different CO_2 fire and NEE priors assimilating: i) OCO-2 XCO_2 retrievals and ii) CO_2 in-situ data. See redtable **??** Fig. 2 for details of the eight CO_2 inversions.

To investigate the uncertainty in inferred CO_2 emissions arising from the selection of fires, we perform CO_2 inversions with three different global gridded fire estimates. The first one is taken from the GEOS-Carb CASA-GFED3 product (Ott2020), which we label “FIRE3"; for the second we use GFED4.1s, denoted “FIRE4". The third set, described in Section 2.3.1.b and denoted “FIREMo", is created by first optimizing CO emissions with MOPITT observations and then converting them to CO_2 emissions using the landcover ratios and parameters in GFED4.1s. The methodological differences between FIRE3 (GFED3) and FIRE4(GFED4.1s) are described in section 2.3.1.a. Figure A1 S2 shows annual differences between FIRE3 and FIRE4 from 2015 through 2018 over the OCO-2 MIP regions. We note that regional differences are as large as 140 TgC per year, or roughly $\sim$10% of the annual global fire emissions budget which has been estimated to 1.6 $\pm$ 0.7 GtC/yr (Friedlingstein2020). Additionally, the size and sign of the differences varies by year and by region. For instance, FIRE3 (GFED3) generally predicts higher CO_2 emissions over the Boreal regions, while FIRE4 (GFED4.1s) largely predicts more fire emissions from the Northern midlatitudes. This is consistent with differences between the two models, i.e. GFED4.1s uses a different set of emission factors separating trace gas emissions and aerosol from boreal forest to temperate forests (Akagi2011, VanderWerf2017). VanderWerf2017 have shown that GFED3 does not capture the different patterns of fire severity between the boreal regions of north America and Eurasia and the differences between boreal and temperate forests fires (which could explain the large difference between FIRE4 and FIRE3 in Fig.A1 S2). In addition, VanderWerf2017 found that including small fire burned area in GFED4 doubled the burned area in temperate north America and Europe compared to GFED3. Interestingly, the differences in the tropics have a pronounced meridional zonal structure, where GFED4.1s predicts smaller emissions in south America, tropical Asia, and north Africa (after 2016), and larger emissions in southern tropical Africa. The addition of small fire burned area included in GFED4.1s has a strong impact in the southern tropical Africa regions where agricultural waste burning and shifting cultivation are important drivers of fire activity. VanderWerf2017 have shown that the increase of

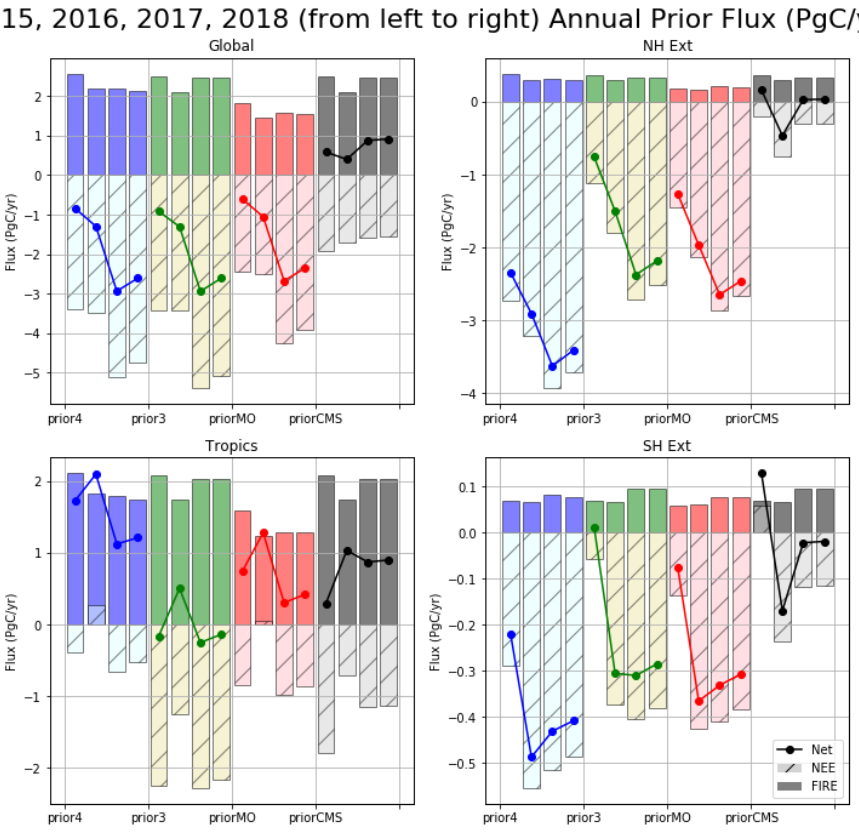

Figure 5. Annual prior CO_2 emissions, in global and by latitude bands, used later in top-down inversions. Annual net flux (lines), NEE (bars with hatches) and FIRE (bars with darker colors) prior emissions are represented from 2015 through 2018 (left to right) between GFED4.1s (blue), GFED3 (green), MOPITTopt (red) and CMS (black).

burned area in these regions were associated with small fire burned area from the last GFED version. Small fires linked with deforestation and agricultural waste are also important over the Indonesia, however deforestation activity decreased of almost 50% in 2017 and 2018 thanks to several Indonesian policies in order to prevent forest fires and land clearing with particularly the new law avoiding to clear forest for oil palm plantations (GlobalForestWatch2020). This might explain the decrease in fire emissions over southern tropical Asia in 2017 and 2018 with GFED4.1s, in addition that 2017 and 2018 were not impacted by the 2015 El Niño event where large fires burned in Indonesia.

3.2.1 Prior NEE and fires CO_2 fluxes

At latitude scale, we can see that the non-CMS priors give more net sinks in the Northern (between -1 PgC/yr and -4 PgC/yr) and Southern Hemispheres Extra-Tropics, while CMS has lower values and even net sources in 2015 for both hemispheres and in 2018 as well for the Northern Hemisphere. These differences between the priors is also observed for the Northern and

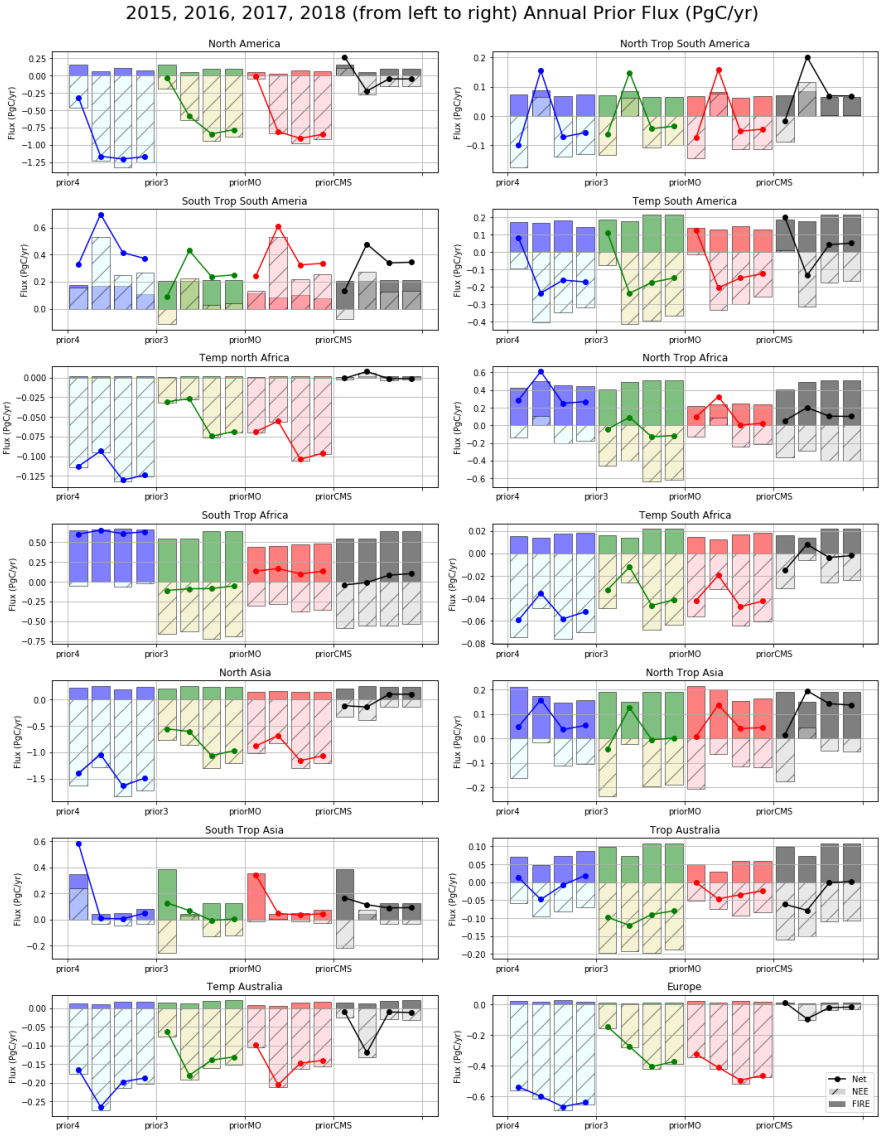

Figure 6. Same as Fig. 5 but for the OCO-2 MIP regions.

Southern Hemisphere OCO-2 MIP regions (Fig. **??**). In addition, we can observe that GFED4 and MOPITTopt priors have a deeper Northern Hemisphere sinks than GFED3 (particularly observed for Europe and Northern Asia, Fig. **??** and Fig. 6 and Fig. **??**), which is balanced by stronger net sources over the Tropics (coming mainly from Southern Tropical Africa and Southern Tropical Asia respectively, Fig. **??**). For Tropical South Africa, we can see a discrepancy in the zonal flux distribution between GFED3 and, GFED4 and MOPITTopt which could result due to the adjustment and modification of the respiration with the fires for GFED4 and MOPITTopt which is not considered for GFED3 as we took the fire and respiration directly from CMS (GEOS-Carb). The scaling of GFED3 GPP and respiration to match the global AGR yields deeper biogenic sinks over the Tropics than with all the other priors. We can also observed for Southern Tropical Africa that FIRE4 has larger fires than FIREMo, consistent with the fact that GFFED4.1s CO was observing higher CO fire emissions than MOPITT (Fig. 4 and Fig. **??**)

In addition, the global fires emissions indicate that FIREMo observes less emissions compared to all other priors, a difference coming from tropical regions. These lower fire emissions observed by FIREMo in the Tropics come mainly from Tropical Australia (with values in 2015 of $\sim$0.05 PgC/yr for FIREMo compared to $\sim$0.07 PgC/yr for FIRE4 and $\sim$0.095 PgC/yr for FIRE3), Tropical Africa ($\sim$0.35 PgC/yr, $\sim$0.50 PgC/yr, $\sim$0.55 PgC/yr respectively for FIREMo, FIRE4 and FIRE3) and Southern Tropical South America ($\sim$0.1 PgC/yr, $\sim$0.17 PgC/yr, $\sim$0.2 PgC/yr respectively for FIREMo, FIRE4 and FIRE3). Characteristics that came with the differences between GFED4.1s CO and MOPITT CO fire emissions (see Fig.4 and Fig.**??**). But we observe a larger fire emissions with FIREMo in Southern Tropical Asia (fire emissions of $\sim$0.37 PgC/yr for FIREMo compared to $\sim$0.35 PgC/yr for FIRE4) and in Northern Tropical Asia ($\sim$0.22 PgC/yr for FIREMo, $\sim$0.21 PgC/yr for FIRE4, and $\sim$0.19 PgC/yr for FIRE3).

We can then see the impact of including MOPITT CO data in the CO_2 fire priors compared to the emission inventories known to have biased carbon emissions in Tropical Asia. The larger emissions with FIREMo compared to FIRE4 over tropical Asia comes mainly from some specific vegetation. The main vegetation type in this region is savanna and we can observe that for the CO_2 prior emissions, FIREMo has the higher flux for Northern tropical Asia (Southern tropical Asia) compared to FIRE3 and FIRE4 (FIRE4 respectively) for savanna but also for agriculture and deforestation (see Fig. **??**). Another impact of including CO MOPITT data in the CO_2 fire priors appears in variability. As already observed with the CO emissions (Fig. **??**) and discussed in VanderLaan-Luijkx2015 and Nechita-banda2018, the seasonality of fires over tropical Asia is better captured with MOPITT than with the emission inventories for peat lands. However, this is not only true for peat but also for other vegetation types. For savanna, agriculture and peat lands, FIREMo observed a peak in fire seasonality after the peaks observed with the GFED (Fig. **??**). This is particularly true for the 2015 El Niño fires but less for the fires that occurred in 2017 and 2018. In this period, FIREMO does not observed as much fire emissions as the GFED with a similar seasonality. The difference in seasonality for 2015 could be a result of the large and intense fires during the El Niño event burning larger regions and releasing more smokes which could have impacted the MODIS burned area data used in GFED but probably also the MOPITT retrievals. Further investigation are then needed to study this region.

We can observe that GFED4 and MOPITTopt priors have a deeper Northern Hemisphere sinks than GFED3 (particularly observed for Europe and Northern Asia, Fig. **??** and Fig. 5 and Fig. 5), which is balanced by stronger net sources over the

Tropics (coming mainly from Southern Tropical Africa and Southern Tropical Asia respectively (Fig. **??**). The scaling of GFED3 GPP and respiration to match the global AGR yields deeper biogenic sinks over the Tropics than with all the other priors. We can also observe for Southern Tropical Africa that FIRE4 has larger fires than FIREMo, consistent with the fact that GFFED4.1s CO was observing higher CO fire emissions than MOPITT (Fig. 4 and Fig. **??**).

The global fire emissions indicate that FIREMo yields less emissions compared to all other priors, a difference coming from tropical regions. These lower fire emissions observed by FIREMo in the Tropics come mainly from Tropical Australia (with values in 2015 of ∼0.05 PgC/yr), Tropical Africa (∼0.35 PgC/yr) and Southern Tropical South America (∼0.1 PgC/yr). Characteristics that came with the differences between GFED4.1s CO and MOPITT CO fire emissions (see Fig.4 and Fig.**??**). But larger fire emissions are observed with FIREMo in Southern and northern Tropical Asia compared to FIRE4. The larger emissions with FIREMo compared to FIRE4 over tropical Asia comes mainly from savanna (the main vegetation type in this region, see Fig. **??**).

As already observed with the CO emissions (Fig. **??**) and discussed in VanderLaan-Luijkx2015 and Nechita-banda2018, the seasonality of fires over tropical Asia is better captured with MOPITT than with the emission inventories for peat lands. However, this is not only true for peat but also for other vegetation types. For savanna, agriculture and peat lands, FIREMo observed a peak in fire seasonality after the peaks observed with GFED (Fig. **??**). This is particularly true for the 2015 El Niño fires but less for the fires that occurred in 2017 and 2018. In this period, FIREMO does not observed as much fire emissions as GFED with a similar seasonality. The difference in seasonality for 2015 could be a result of the large and intense fires during the El Niño event burning larger regions and releasing more smoke which could have impacted the MODIS burned area data used in GFED but probably also the MOPITT retrievals. Further investigation are then needed to study this region.

3.2.2 Comparison between the CO_2 posterior fire and biospheric emissions : impact of re-balanced NEE and fire prior in CO_2 posterior emissions

We assimilated OCO-2 and in situ data separately in order to assess the impact of these data in conjunction with different fire emissions and corresponding land flux priors. In all inversions, only NEE and ocean fluxes have been optimized.

a) Global and latitudinal flux

Figure 7 shows global and latitudinal annual net fluxes, FIRE and NEE fluxes for both OCO-2 and in situ inversions. We can see that globally, net fluxes for OCO-2 posterior emissions across the different priors are consistent. The sinks seem to adjust the different fire contributions. This is also observed for the in situ inversions. The in situ inversions give, compared to OCO-2 inversions, a $\sim$ 1 PgC/yr deeper net sink in 2015 and 2016, and a $\sim$ 2PgC/yr deeper net sink for 2017 and 2018, which originates from a weaker source (or sink) in the Tropical regions than the OCO-2 informed inversions. These differences are in agreement with the differences between OCO-2 and IS inversions the larger ensemble of inversions detailed in (Crowell2019) and (Peiro2022).

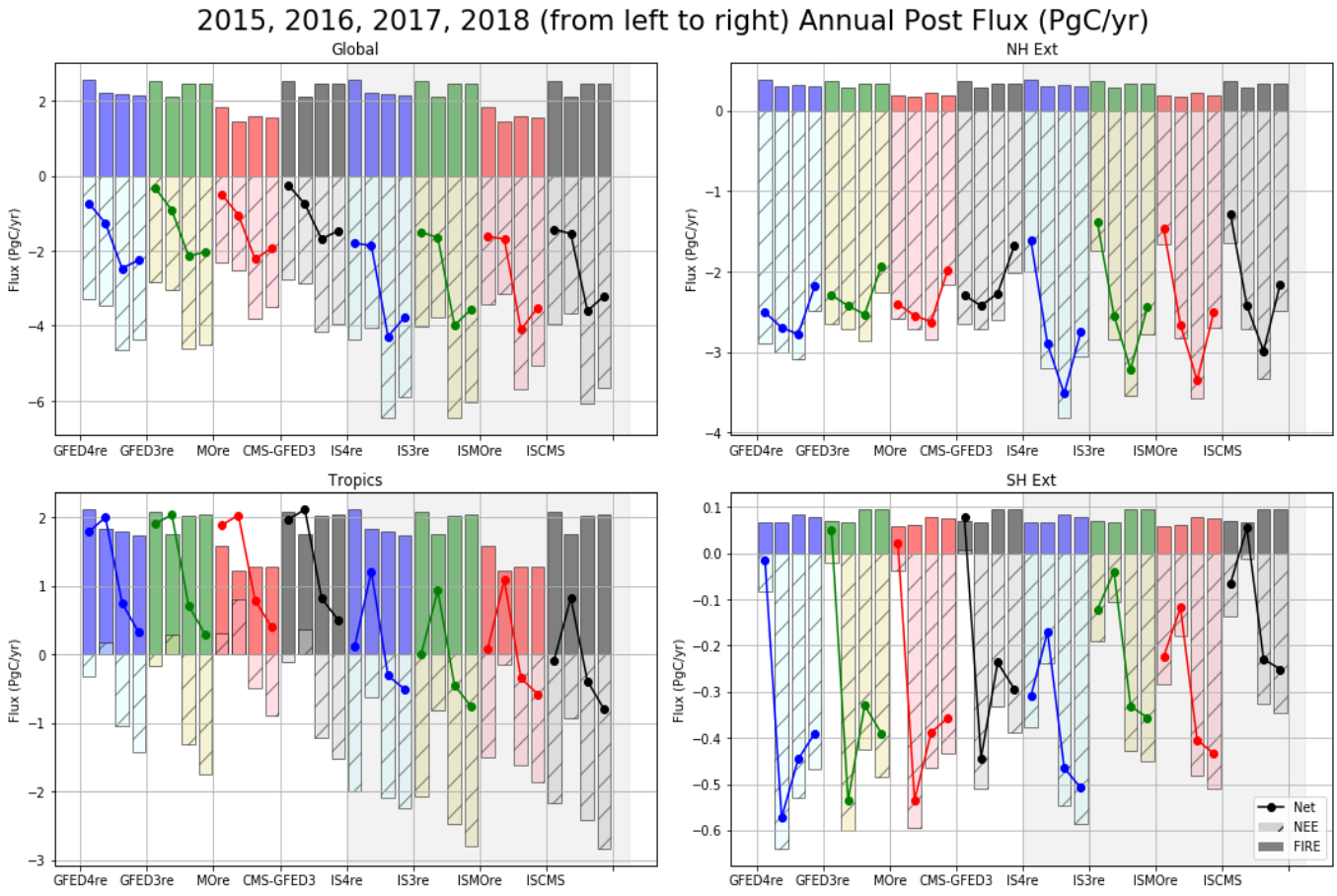

Figure 7. Global and latitudinal CO_2 posterior emissions between OCO-2 and in situ inversions as GFED4re (in blue), GFED3re (in green), CMS (in black) and MOre (in red). Annual fluxes are displayed from 2015 (left) through 2018 (right). FIRE emissions are darker colored bars, NEE fluxes are hatched bars and lines depict the net land fluxes.

The Northern Hemisphere Extra-Tropics (NH Ext) posterior fluxes are consistent across the different priors for both observation constraints, which is not surprising given the good coverage of the in situ observations in this region. For OCO-2 inversions, we can see small variations from year to year (going to -2.5 PgC/yr in 2015 through -2.75 PgC/yr in 2016) except for 2018 where the net sink drops to -2 PgC/yr. The net sinks observed with the in situ inversions are weaker than OCO-2 for 2016, 2017, and 2018, and the year-to-year variations are significantly larger than the OCO-2 results. Similar behavior is observed for the SH Ext and opposite behavior for the Tropics with larger sources for the OCO-2 inversions, which could be related to cross-talk between the zonal bands given the sparse coverage of in situ data in the Tropics. However the net fluxes are closer between in situ and OCO-2 inversions over the NH Ext than for the Tropics, where the in situ fluxes are generally 1-1.5 PgC less than the OCO-2 fluxes. The consistency across the priors for the Northern latitude bands are also observed in the simulation study of Philip2019 where they used different NEE priors to observe the impact on the OCO-2 posteriors.

Comparing the posterior emissions (Fig. 7) with the prior emissions (Fig. 5), we can see an impact from the observations assimilated on the CMS prior which shift significantly toward the other posterior fluxes at global and latitudinal scales. CMS posterior emissions seem to have slightly weaker sinks than the posterior using the rebalanced priors. The imposed AGR seems then to have an impact at latitudinal scales. For the Tropics, we can again observe a consistency in OCO-2 across the priors. MOre and ISMOre have a smaller sink in 2015 (with sources for OCO-2 inversion) compared to the other inversions in order to balance the 0.5 PgC/yr smaller fires that FIREMo gives. This balance was also observed for the priors (see Fig. **??**). The range of net flux observed with all OCO-2 inversions are consistent with other studies (Palmer2019, Crowell2019). Further, the intense fires and CO_2 sources related to the 2015 El Niño Oscillation over the Tropics and mainly Indonesia might not be seen with in situ data due to their weak coverage in these regions. This could then explain why we observe stronger sinks with in situ than OCO-2 posterior NEE emissions. Comparing the OCO-2 inversions with the *in-situ* ones shows that the in situ net fluxes are totally different with a Tropical sink in all years except in 2015 and 2016 which has a net source. 2017 and 2018 are particularly strong sinks of $\sim$ -0.5 PgC/yr. These deeper sinks would explain part of the larger global sink from the in situ inversions. We will see in the next subsection that these sinks with in situ are coming from the Northern Tropical regions such as Northern Tropical Africa and Northern Tropical Asia (see Fig. 8 and Fig. **??**). As observed for the previous Extra-Tropical band, SH Ext shows similar fluxes across the priors for each data constraint. However 2016 is adjusted downward significantly for the OCO-2 fluxes (between -0.4 PgC/yr and -0.6 PgC/yr) compared to the in situ fluxes (between -0.2 PgC/yr and 0.1 PgC/yr). In addition, while OCO-2 net fluxes have stronger sources in 2016 over the Tropics, they have a deeper sinks over the SH Ext than with the in situ fluxes. This result suggest a transport connection between the Tropics and SH Ext fluxes with the OCO-2 inversions, where land coverage is limited and hence retrievals are sparser than the other regions. On the other hand, this does not seem to be the case in the in situ results, but we know that there are a few in situ data present in the SH Ext and so they have a different data constraint. The MOPITT results look like the GFED4.1s results for the Tropical regions, while the GFED3 and CMS results look alike, suggesting the sensitivity in these regions to the fire prior, not only for IS but also for OCO-2 data constraint.

Figure 7 shows global and latitudinal annual net fluxes, FIRE and NEE fluxes for both OCO-2 and in situ inversions. We can see that globally, net fluxes for OCO-2 posterior emissions across the different priors are consistent. The sinks seem to adjust the different fire contributions. This is also observed for the in situ inversions. The range of net flux observed with all OCO-2 inversions are consistent with other studies Palmer2019, Crowell2019, Peiro2022. Global sinks are larger with IS inversions than with OCO-2 ones. These sinks observed with in situ are driven by larger sinks in the tropics (Fig. 7). CMS-GFED3 and ISCMS posterior emissions seem to have slightly weaker sinks than the other posteriors. The imposed AGR seems then to have an impact at latitudinal scales. The Northern Hemisphere Extra-Tropics (NH Ext) posterior fluxes are consistent across the different priors for both observation constraints, which is not surprising given the good coverage of the in situ observations in this region. The consistency across the priors for the Northern latitude bands are also observed in the simulation study of Philip2019 where they used different NEE priors to observe the impact on the OCO-2 posteriors. For OCO-2 inversions, we can see small variations from year to year (going to -2.5 PgC/yr in 2015 through -2.75 PgC/yr in 2016) except for 2018 where the net sink drops to -2 PgC/yr. SH Ext shows similar fluxes across the priors for each data constraint. However 2016 is adjusted

downward significantly for the OCO-2 fluxes (between -0.4 PgC/yr and -0.6 PgC/yr) compared to the in situ fluxes (between -0.2 PgC/yr and 0.1 PgC/yr), balanced with stronger sources over the Tropics. This result suggest a transport connection between the Tropics and SH Ext fluxes with the OCO-2 inversions, where land coverage is limited and hence retrievals are sparser than the other regions. On the other hand, this does not seem to be the case in the in situ results, but we know that there are a few in situ data present in the SH Ext and so they have a different data constraint. For the Tropics, we can again observe a consistency in OCO-2 across the priors. The intense fires and CO_2 sources related to the 2015 El Niño Oscillation over the Tropics and mainly Indonesia might not be seen with in situ data due to their weak coverage in these regions. This could then explain the larger sinks with in situ NEE emissions. Even though we observe a consistency across the priors, MOre and ISMOre have a smaller sink in 2015 (with sources for OCO-2 inversion) compared to the other inversions in order to balance the 0.5 PgC/yr smaller fires that FIREMo gives. This balance was also observed for the priors (see Fig. **??**). The net fluxes of ISMOre and IS4re look similar for the Tropical regions, while the net fluxes of IS3re and ISCMS look alike, suggesting the sensitivity in these regions to the fire prior, not only for IS but also for OCO-2 data constraint.

b) Regional fluxes

When we compare the posterior regional fluxes, we can see difference in the carbon balance. If we first look the Northern Extra-Tropical regions (North America, North Asia and Europe), we can see that the OCO-2 inversions have deeper net sinks over the boreal regions than with IS (see Fig. **??**). The in situ data are placing almost all of the NH Ext sink over Northern Asia, but are placing sources of carbon over North America for 2015. OCO-2 only sees net sinks of carbon for all NH Ext. In-situ data do not have an homogenize coverage over the NH Ext band : large number of observations are situated over Temperate North America and Europe but are very sparse over the Boreal regions and Temperate Eurasia (see Fig. **??**). The large differences in net sinks occur then over the regions with few data (Boreal and Eurasia regions). It is interesting also to see balance between the regions in Northern Hemisphere with Southern Hemisphere. For instance, it seems that the drop off sinks (starting in 2017 and so representing the "recovery" period) observed with both IS and OCO-2 over North Asia is balanced by the Tropical Asia (North and South) where net fluxes go from sources to sinks. 2015 was a large net sources of carbon (due to intense fires) while 2016, 2017 and 2018 are deeper sinks with IS over Northern Tropical Asia and sinks with OCO-2 over Southern Tropical Asia . At the same time, posterior fluxes in Europe are anti-correlated with posterior fluxes over Northern Tropical Africa. The deeper sinks observed with OCO-2 in Europe are anti-correlated with the net sources observed in Northern Tropical Africa , where the post ENSO period has smaller sources in Northern Tropical Africa linked with smaller sinks in Europe (Fig. 8). Emissions estimated observed with OCO-2 are more in line with previous studies even though the years of study were before 2015. Reuter2014 found, using GOSAT data, uptake of carbon per year around 1 PgC/yr which was 0.5 PgC/yr higher than expected from in situ inversions. However, as mentioned in Reuter2017, there is a lack of carbon budget information over Europe and there is hence no estimate that can be refuted at present .

We then can see that this deeper sinks in the NH Ext with OCO-2 are in fact balanced by the Tropics. The weaker net sink observed with IS compared to satellite data was also observed with Houweling2015a who were using GOSAT retrievals

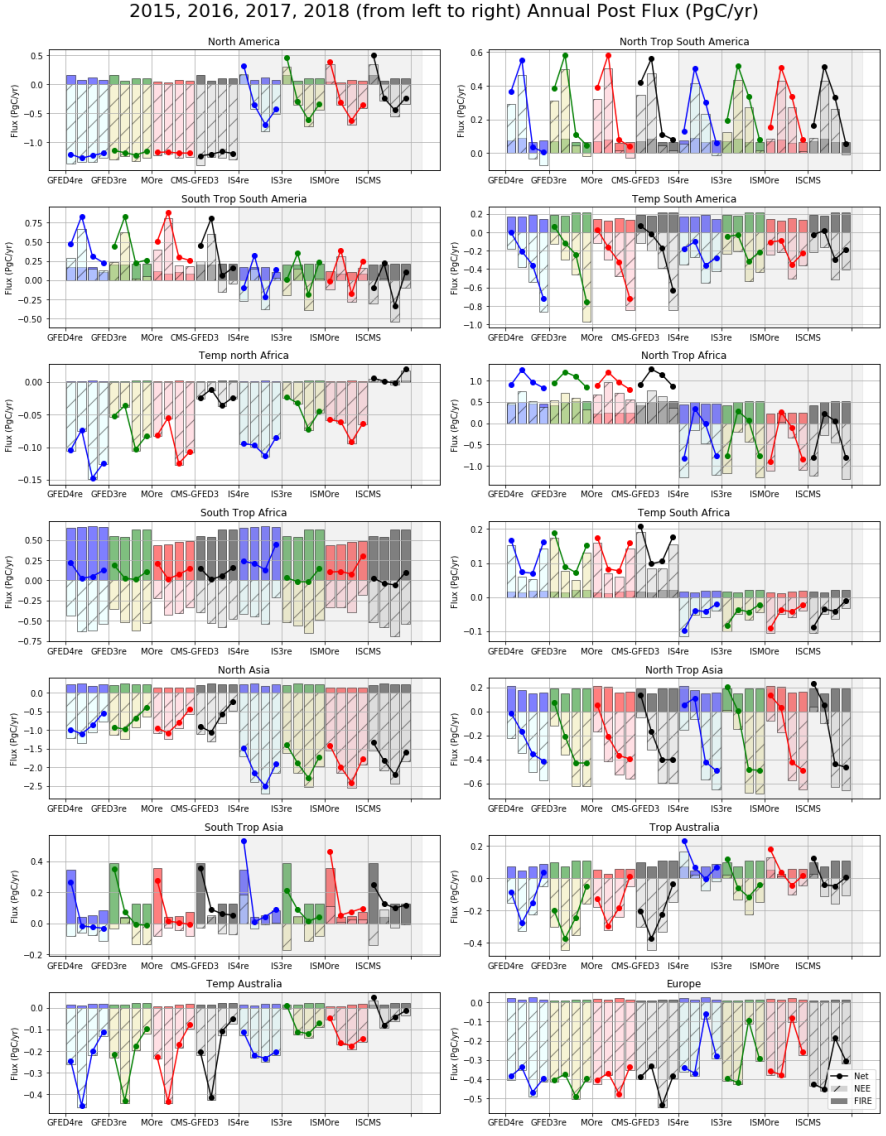

Figure 8. Same as Fig. 7 but for all OCO-2 MIP regions (from left to right, top to bottom) : north America, North Tropical South America, South Tropical South America, Temperate South America, Temperate North Africa, North Tropical Africa, South Tropical Africa, Temperate South Africa, north Asia, North Tropical Asia, South Tropical Asia, Tropical Australia, Temperate Australia, and Europe.

instead of OCO-2 for the 2009-2010 period. Additionally, what is observed here between IS and OCO-2 inversions was also observed in the study of Peiro2022 who found that by using OCO-2 v9 the inversions showed weaker sinks over Northern Asia but a deeper sink over Europe and Northern America than with the in situ inversions. We can see that our inversions here are within the estimates observed in the study of Peiro2022. However, for Europe, we can see that the variability in our priors is different than the ones used in Peiro2022. Our re-balanced priors give the deepest sink in 2017 (in 2016 for CMS prior) which is observed as well in the posteriors net fluxes using OCO-2 and it is in opposition of the OCO-2 inversions of Peiro2022 which have deeper sinks in 2016. This is due to stronger fire emissions in 2017 compared to the other years balanced with the respiration, and the differences between the two studies could be due to the re-balanced respiration.

In average for all regions, we can see a disagreement between IS and OCO-2 inversions but an agreement across priors within each observational constraint. Additionally, comparing the different priors, we can see that inversions using the FIREMo are closer to the ones using FIRE4 while CMS is closer to the inversions using FIRE3, i.e. the fires seem to have more impact than the rebalancing to match the global AGR. We can observe that for almost all regions, the sinks with NEE4 and NEEMo are deeper than with NEE3 and CMS but they are balanced with higher sources for the other regions that have net sources, regions mainly over the Tropics.

Focusing on the Tropical regions, we can first see that for Northern Tropical South America (Fig. **??**), OCO-2 fluxes are consistent for each priors used with around 0.5 PgC/yr efflux during the El Niño period (2015-2016) and neutral emissions during the recovery period. IS fluxes are also strong during the El Niño period, but remain moderately high in 2017. As observed in the Fig. 1 of the paper of Peiro2022, which used the same set of IS data, the number of IS data does not decrease significantly, meaning that changing observational coverage is not the cause of this behavior. One possible explanation is the lag between flux in the Tropics and observation by the in situ network, which could be aliasing flux signals in time, though this hypothesis is difficult to test. For Northern Tropical Africa (Fig. 8), as already mentioned above, large difference are seen between OCO-2 and IS inversions. OCO-2 net fluxes are strong with high sources of carbon between 0.5 PgC/yr and 1.5 PgC/yr. We can see also some fire-dependent differences : FIREMo and FIRE4 drop off for 2017 but FIRE3 driven fluxes do not. This difference in 2017 is particularly observed with OCO-2. IS, on the contrary, give strong sinks in this region, the strongest one for all Tropical regions. Examining Fig. **??**, we note the dependence of the IS posterior emissions known with the priors. Northern Tropical Africa is known to have very few IS data compared to the other Tropical regions (Fig. **??**). Northern Tropical Asia (Fig. **??**) shows agreements between the priors and OCO-2 data constraints for 2015 and 2016, but shows significant differences between OCO-2 and IS for 2017 and 2018. The IS and OCO-2 inversions all agree together that there is a source of carbon in 2015 but OCO-2 inversions have a smaller sink in 2016 while it is a source with IS (smaller with IS3re and IScms), which seems to show an impact of the El Niño event and impact of the fire priors with IS, while for 2017 and 2018, IS particularly seems to show a stronger recovery in the region than observed by OCO-2. The sparse coverage of in-situ data over this region could explain the difference with OCO-2, though not specifically for 2017 alone, and hence further investigations are needed for this region.

Very large differences between the IS and OCO-2 inversions appears for Southern Tropical South America (Fig. **??**) as well. Interestingly, the OCO-2 posteriors emissions seem to be closer to the priors than the IS are. One explanation for that has

been mentioned previously in Peiro2022, where the cloud coverage above the moist Amazon decreases the amount of OCO-2 retrievals, while IS data are located more inside the moist Amazon. This difference in posterior flux could then come from different area of observation. In opposition to the other Southern Tropical regions, the ENSO signal appears in 2016 instead of 2015 for OCO-2. This region follows the inter-seasonal variations of the Northern Tropical regions, which also see highest emissions in 2016.

Southern Tropical Africa is almost neutral in the OCO-2 posterior fluxes (see Fig. **??**). We can see the large balance between the intense fires and the respiration, which are anti-correlated in their variability. GFED4re and MOre have larger sources than GFED3re and CMS. With the IS, there is large variation across the priors where IS4re and ISMOre both constrain a source of carbon for the whole period, while ISCMS and IS3re have smaller source of carbon and even a sink in 2016 and 2017. These differences seem to suggest that both fires and respiration are especially important when observational coverage is limited.

Finally, Southern Tropical Asia (Fig. **??**) shows difference among the prior ensemble for both OCO-2 and IS inversions with particularly differences in the fires for 2015. The inversions adjusted the sinks for the MOre and GFED4re inversions to be larger than the two other inversions in order to accommodate the smaller fires observed with FIREMo and FIRE4. This is not observed however for the IS inversions which just show sources of carbon for both ISMOre and IS4re while the inversions constrained with the GFED3 fires (IS3re and IScms) give sinks of carbon showing smaller net carbon. The impact of the fires over this region seems to have a strong impact with both data constraint. The IS inversions using FIREMo and FIRE4 show then large sources in 2015, which are not observed with FIRE. If we compare the posteriors with the priors, we can in fact see that the IS tends to be closer to the priors than the OCO-2 inversions. This suggest that for this region as well, the few amount of IS data might explain this result and the larger amount of OCO-2 seems to better constrain the posterior fluxes.

In summary, we observe consistent differences between the Northern latitudinal regions and the Tropics, where the respiration tends to be higher over the Northern latitudes than the Tropics (which has larger sources), and IS has higher NEE than OCO-2. Differences in the priors used show impact particularly over the Tropics where both GFED4 and MOPITT observe large fires emissions. The MOPITT results look like the GFED4.1s results for the Southern Tropical regions, while the GFED3 and CMS results look alike, suggesting the sensitivity in these regions to the fire prior, not only for IS but also for OCO-2 data constraint.

When we compare the posterior regional fluxes, we can see difference in the carbon balance.

If we first look the Northern Extra-Tropical regions (North America, North Asia and Europe), we can see that the OCO-2 inversions have deeper net sinks than IS (see Fig. **??**). The in situ data are placing almost all of the NH Ext sink over Northern Asia, while there are sources of carbon over North America for 2015. In-situ data do not have an homogenize coverage over the NH Ext band: large number of observations are situated over Temperate North America and Europe but are very sparse over the Boreal regions and Temperate Eurasia (see Fig. **??**). The large differences in net sinks occur then over the regions with few data (north Asia regions).

It is interesting also to see balance between the regions in Northern Hemisphere with Southern Hemisphere. For instance, it seems that the sink decreased for 2018 (starting in 2017) observed with both IS and OCO-2 over North Asia is balanced by net sinks in tropical Asia (North and South). The deeper sinks observed with OCO-2 in Europe are also anti-correlated with the net

sources observed in Northern Tropical Africa (Fig. 7). Reuter2014 found a similar mass balance, using GOSAT data, uptake of around 1 PgC/yr which was 0.5 PgC/yr higher than expected from in situ inversions. However, as mentioned in Reuter2017, there is a lack of carbon budget information over Europe and there is hence no reliable benchmark for comparison. The balance observed here between IS and OCO-2 inversions was also observed in the study of Peiro2022. However, for Europe, we can see that the variability in our priors is different than the ones used in Peiro2022. A major difference between this study and Peiro2022 is that the rebalanced priors and posterior fluxes provide the largest sink in 2017, as opposed to 2016. This is likely a consequence of the larger fires and the subsequent rebalanced respiration that was derived in our study.

Across the different fire emissions we observe a split: MOre and GFED4re inversions (respectively ISMOre and IS4re) are similar, while GFED3re and CMS-GFED3 (respectively IS3re and ISCMS) are more similar. That means fires have a larger impact on the posterior solution than the rebalancing of prior NEE to match the global AGR. We can observe that for almost all regions, the sinks with NEE4re and NEEMore are deeper than with NEE3re and Geos-Carb CMS but are balanced with larger sources in other regions, mainly over the Tropics (Fig. 7).

Focusing on the Tropical regions, OCO-2 fluxes are consistent for each priors. For Northern Tropical South America (Fig. 7), OCO-2 fluxes have around 0.5 PgC/yr efflux during the El Niño period (2015-2016) and neutral emissions during the recovery period. IS fluxes are also strong during the El Niño period, but remain moderately high in 2017. As observed in the Fig. 1 of the paper of Peiro2022, which used the same set of IS data, the number of IS data does not decrease significantly, meaning that changing observational coverage is not the cause of this behavior. The number of in situ observation is particularly low in the tropics compared to the extra-tropical southern and northern hemispheres (Fig. 2 of Peiro2022). One possible explanation is the lag between flux in the Tropics and observation coverage by the in situ network, which could be aliasing flux signals in time, though this hypothesis is difficult to test. Very large differences between the IS and OCO-2 inversions appears for Southern Tropical South America (Fig. 7). The OCO-2 posteriors emissions seem to be closer to the priors than the IS are. One explanation for that has been mentioned previously in Peiro2022. The cloud coverage above the moist Amazon decreases the amount of OCO-2 retrievals, while IS data are located more inside the moist Amazon. This difference in posterior flux could then come from different area of observation. In opposition to the other Southern Tropical regions, the ENSO signal appears in 2016 instead of 2015 for OCO-2. This region follows the inter-seasonal variations of the Northern Tropical regions, which also see highest emissions in 2016.

For Northern Tropical Africa, OCO-2 net fluxes are strong with high sources of carbon between 0.5 PgC/yr and 1.5 PgC/yr. We can see also some fire-dependent differences : FIREMo and FIRE4 sinks decrease for 2017 but FIRE3 driven fluxes do not. This difference in 2017 is particularly observed with OCO-2. IS, on the contrary, give strong sinks in this region, the strongest one for all Tropical regions. Examining Fig. **??**, we note the known dependence of the IS posterior emissions with the priors. Northern Tropical Africa is known to have very few IS data compared to the other Tropical regions (Fig. **??**). For southern Tropical Africa, we can see the large balance between the fires and the respiration, which are anti-correlated in their variability. GFED4re and MOre have larger sources than GFED3re and CMS-GFED3. With the IS, there is large variation across the priors where IS4re and ISMOre both constrain a source of carbon for the whole period, while ISCMS and IS3re have smaller source

of carbon and even a sink in 2016 and 2017. These differences seem to suggest that both fires and respiration are especially important when observational coverage is limited.

Northern Tropical Asia (Fig. 7) shows agreements between the priors and OCO-2 data constraints for 2015 and 2016, but shows significant differences between OCO-2 and IS for 2017 and 2018. The sparse coverage of in-situ data over this region could explain the difference with OCO-2, though not specifically for 2017 alone, and hence further investigations are needed for this region. Finally, for southern Tropical Asi, the inversions adjusted the NEE sinks for MOre and GFED4re inversions to be larger than the two other inversions in order to accommodate the smaller fires observed with FIREMo and FIRE4. This is not observed however for the IS inversions which just show NEE sources for both ISMOre and IS4re. The impact of the fires over this region seems to have a strong impact with both data constraint. If we compare the posteriors with the priors, we can in fact see that the IS tends to be closer to the priors than the OCO-2 inversions. This suggest that for this region as well, the few amount of IS data might explain this result and the larger amount of OCO-2 seems to better constrain the posterior fluxes.

In summary, we observe consistent differences in posterior NEE between IS and OCO-2 inversions. Some of these differences are caused by differences in data coverage and cloud fraction. For all data constraints, we can observe a smaller sinks in the tropics during El Nino, while larger net sinks are observed in the NH Ext. Moreover, larger sinks are observed with OCO-2 in north America and Europe, while larger sinks are observed with IS in Asia. Finally, the net fluxes using FIREMO look like those using FIRE4 for the southern tropical regions, while net fluxes using FIRE3 look alike, suggesting the sensitivity in these regions to the fire prior, not only for IS but also for OCO-2 data constraint.

3.2.3 Evaluation of the simulations

3.2.3.a Evaluation of the inversions to fit the OCO-2 retrievals and IS data

The global distributions of OCO-2 retrievals over the 2015-2018 period (Fig. 9.a) shows a latitudinal gradients from north to south with higher XCO_2 concentrations in the tropics and the northern hemisphere. High land values (no higher than 409 ppm) are observed over east Asia, north west Africa, and north tropical south America. Figure. 9.b shows the global distributions of IS data with higher number of observations in the northern hemisphere than the tropics or the southern hemisphere. High XCO_2 concentrations (higher than 409 ppm) can be observed for temperate north America and near the coast of east Asia. The regional mean differences between the prior or posterior and the OCO-2 retrievals (IS data) are summarized in Table S1.

The prior have larger differences with the OCO-2 retrievals than the posteriors. The prior3 (using both FIRE3 and NEEre3, see Fig. 2) better fit the OCO-2 measurements than the other priors for the southern hemisphere and the tropics (Fig. 9 and Table S1). The priorCMS however does not fit the OCO-2 measurements with high bias between 3 and 4 ppm. The large difference is also observe with the IS measurements. For the IS inversions, the differences between priors and posteriors with the IS data are very similar. This result suggests that the inversion does not change much from the prior, but this result can be explain due to the small number of observations available in these regions. While the optimized concentrations fit the OCO-2 retrievals quite well compared to the priors, suggesting the inversion's ability to fit the data. For the comparison among the simulations, there is no large difference between the different simulations and the data, particularly for the optimized CO_2 measurements.

3.2.3.b Validation against TCCON data

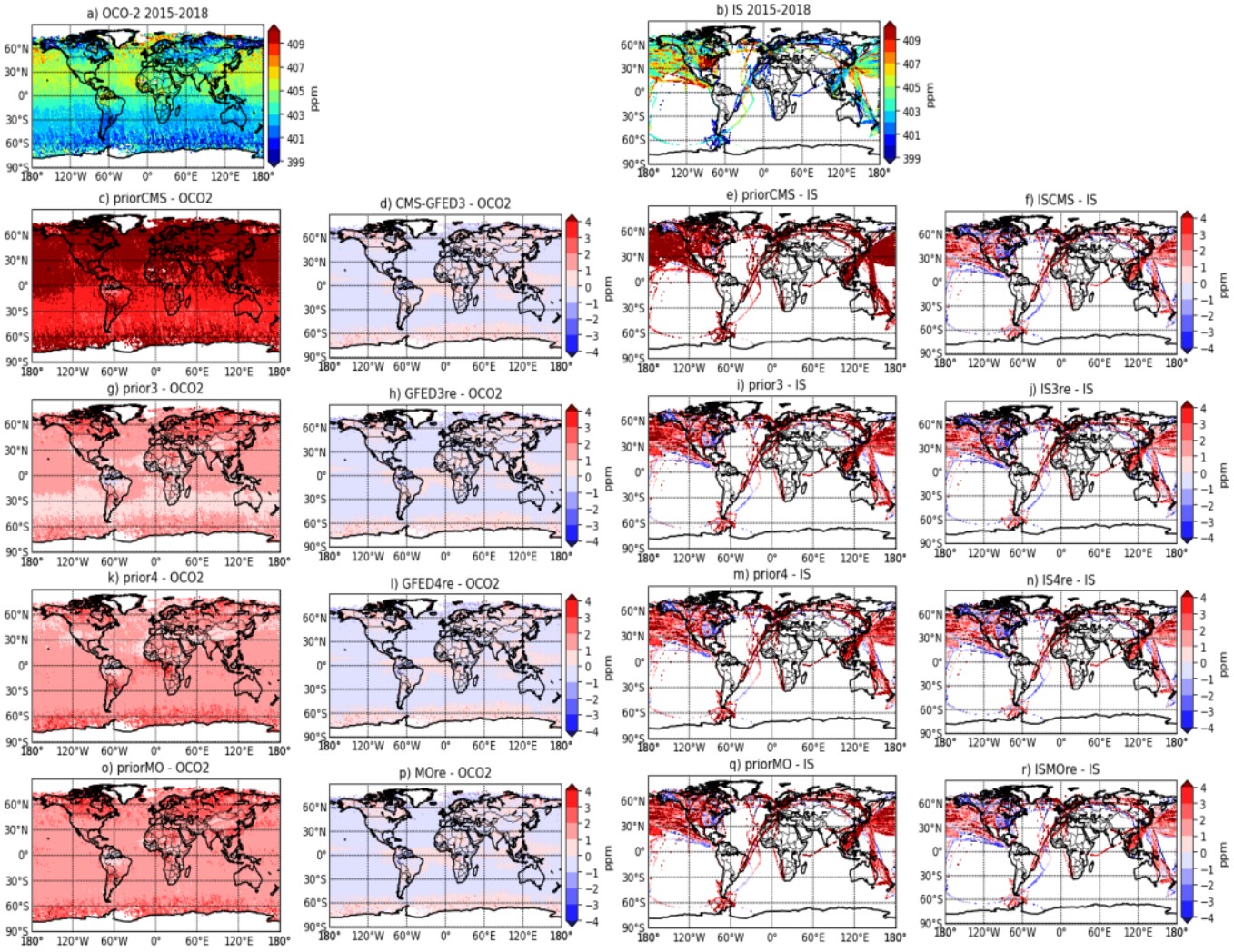

Figure 9. Spatial distributions of the CO2 total column (XCO2). Mean distribution of OCO-2 retrieval (a) and In-Situ data (b) over the 2015-2018 period. Annual difference between the prior of each simulation (CMS (2nd row), prior3 (3rd row), prior4 (4th row) and priorMO (5th row)) and OCO-2 in the 1st column (IS in the 3rd column). Annual difference between the posterior simulation of each simulation (row similar to the priors) and OCO-2 in the 2nd column (IS in the 4th column). Results are in ppm.

As mentioned previously, most of the differences observed between in situ and OCO-2 inversions could be due to their respective coverage. in situ measurements have less data over the Tropics and Southern Hemisphere than OCO-2 retrievals. However, besides the spatial coverage, satellite retrievals might be affected, particularly over the Tropics, by the consistently cloudy region known as the Inter-Tropical Convergence Zone (ITCZ) as well as aerosols from biomass burning or dust (such as over and near the Sahara). It is then important to validate the OCO-2 and in situ posterior simulated mixing ratios against independent data. In this section, in order to explore the accuracy in the posterior fluxes, we evaluated the posterior fluxes by sampling the resultant concentrations for comparison with TCCON measurements. All posterior mixing ratios have been sampled around TCCON retrieval locations and times using the appropriate averaging kernels.

For evaluation of our CO posteriors and priors emissions with TCCON (not shown here), we found that biases between MOPITT CO posterior simulated mixing ratio and TCCON were lower than biases with the CO priors with on average a $\sim$ 5 ppb reduction each year. Additionally, for the 2015-2018 period, the posterior biases were $\sim$ 7 ppb underestimated TCCON values while the priors were $\sim$ 13 ppb overestimated TCCON values. In comparison to TCCON, for the 2015-2018 period, the CO posterior biases were underestimated by 7 ppb, while the CO priors were overestimated by 13 ppb (Fig. S7). Even if the posterior biases are lower than the prior biases, the underestimation observed in Fig. S7 against TCCON could explain the low fluxes observed of the FIREMo compared to the other fire estimates over some regions. We can observe an underestimation of the posterior CO mixing ratio of -12 ppb in 2015 at the Ascension Island site, while the a priori CO mixing ratio has an overestimation of 5 ppb in 2015. However, the biases at the Darwin TCCON site give -3 ppb for 2015-2016 (-0.5 ppb for 2017-2018) with the posterior and 20 ppb for 2015-2016 (22 ppb for 2017-2018) with the prior. This gives the impression that our inversion is not getting the best fluxes for Ascension Island, but we can see that this is not the case for other tropical locations. Ascension Island is known to be impacted with Saharan dust and therefore the posterior simulated concentration could be biased due to aerosols.

Figure 10 shows biases between prior and posteriors simulated mixing ratio (XCO_2) of the different CO_2 inversions against TCCON data by latitudinal bands : Northern Hemisphere Extra-Tropics (NH), Tropics (T), and Southern Hemisphere Extra-Tropics (SH). The number of sites by latitude used for the validation are referenced in the figure caption. The priors used for GFED4re, GFED3re and MOre inversions have similar errors and have particularly less biases over Southern Hemisphere than over the Northern latitudinal (see table **??**). CMS has the largest biases with large XCO_2 overestimation of TCCON values (two times more than biases observed with the three other priors) with biases of 4.82 ppmv in NH and 4.28 ppmv in the Tropics. CMS prior has in addition, the largest standard deviation values compared to the other priors and the lowest coefficient of correlation (table **??**). Improvements of biases and standard deviation with the GFED3re prior compared to CMS which also use FIRE3 as fire prior, are likely due to the re-balanced respiration that match the NOAA growth rate. This re-balanced respiration and growth rate matches have also been used for GFED4re and MOre priors. However, all priors XCO_2 seems to have a positive trend with increase of biases over the time, particularly pronounced for CMS XCO_2. The three mixing ratio of the re-balanced priors are relatively similar, with the MOre prior showing more biases than GFED for the Northern Hemisphere and less biases than GFED4 but more than GFED3 in the Southern Extra-Tropical hemisphere, and almost similar biases than GFED4 in the tropics. However, the tropics have only 3 TCCON sites for validation. Validation over this latitudinal band needs to be viewed

Figure 10. Comparison between TCCON data and the prior (left columns), IS simulations (center columns), and the OCO-2 simulations (right columns). Top panels show experiments biases and bottom panels show standard deviation compared to TCCON sites. Biases and standard deviation are expressed in ppm CO2. For each panel and from left to right are the simulations CMS, GFED3re, GFED4re and MOre.

with this in mind. In Southern Hemisphere, MOre prior has smaller biases than GFED4re. This prior biases improvement might result from the optimized CO fire emissions in the MOre prior, which, has already mentioned, the CO posterior emissions were higher than the CO prior emissions (temperate South Africa and temperate Australia). However the larger biases present in the CO_2 priors with MOPITT fire compared to the GFED priors could come form the underestimation of CO emissions observed with the CO posterior emissions over Boreal forests (CO biases are ∼4ppb lower with XCO posterior than prior for Eureka site but ∼5ppb higher for Ny-Alesund and Sodankyla, not shown here). We observed in the results section that posterior fluxes had similarity across the priors used for each data constraint for SH Ext (see Fig. 7) but 2016 is adjusted downward significantly in the OCO-2 fluxes. We observe, in Fig. 10.l, a larger negative bias for OCO-2 than for IS particularly in 2016. For NH Ext, we observed previously (see Fig. 7 for North America and Europe mainly), a strong sink for OCO-2 over the period compared to IS, which observed stronger year-to-year variability. When evaluating with TCCON data (Fig. 10.j), we can see that OCO-2 has lower biases in 2015-2016 but higher biases for the 2015-2018 period and underestimates the concentration

for almost the whole period compared to IS. The posterior XCO_2 are in better agreement with TCCON measurements than the priors. Additionally, all standard deviation and coefficient of correlation are similar between all inversions with slightly larger standard deviation for the IS inversions than for the OCO-2 inversions. We can also see that all posteriors match the variability of TCCON compared to the priors. Biases observed with CMS have been greatly reduced through the inversion, showing biases of the same order than the other inversions.

Figure 10 shows biases between prior and posteriors simulated mixing ratio (XCO_2) of the different CO_2 inversions against each TCCON sites. While the priorCMS has the largest biases with TCCON and standard deviation, the other priors used (priorCMS, prior3, prior4, and priorMO) have biases and standard deviation very close each other for most of the sites. Improvements of biases and standard deviation with the prior3 compared to priorCMS, which also use FIRE3 as fire prior, are likely due to the re-balanced respiration that match the NOAA growth rate. This re-balanced respiration and growth rate matches have also been used for prior4 and priorMO. While the re-balanced priors mixing ratio are relatively similar, prior4 and priorMO have less biases than prior3. Additionally, depending on the TCCON site, priorMO bias are slightly lower or smaller than prior4. It is then not straight forward to conclude which re-balanced prior is doing better than the others. The posterior XCO_2 are in better agreement with TCCON measurements than the priors. Biases observed with CMS-GFED3 and ISCMS have been greatly reduced through the inversion, compared to priorCMS, with biases of the same order than the other inversions. For the posterior simulated mixing ratio with IS data, we can see that all biases are very similar among the simulations, and it is here again difficult to conclude which posterior do better than the other. On average, IS4re seems to do better but looking site by site, ISMOre can be better than the other simulation (such as for Ascension Island and Reunion Island). Same applies for the posterior simulated mixing ratio with OCO-2 data, where there is not one simulation doing better than the other on average. Additionally, all standard deviation are similar between all inversions with slightly larger standard deviation for the IS inversions than for the OCO-2 inversions. We observed in the results section that posterior fluxes had similarity across the priors used for each data constraint for SH Ext (see Fig. 7) but 2016 is adjusted downward significantly in the OCO-2 fluxes. Evaluation against the two TCCON sites in the SH Ext shows similarity using either IS or OCO-2 constraint (1.3 ppm biases) for Wollongong, but biases are slightly lower with OCO-2 fluxes for Lauder (1.6 ppm with OCO-2 fluxes against 1.7 ppm for IS fluxes). For NH Ext, we observed previously (see Fig. 7 for North America and Europe mainly), a strong sink for OCO-2 over the period compared to IS, which observed stronger year-to-year variability. The evaluation with TCCON data at European sites, shows smaller biases using IS data than OCO-2 data for all simulations. For instance at Garmisch site, biases are around -0.1 ppm and -0.34 ppm with IS fluxes and OCO-2 fluxes respectively, showing a larger underestimation with OCO-2 than IS fluxes. But for the northern American sites, biases are lower with OCO-2 fluxes than IS fluxes (see Lamont site for instance in Fig. 10).

4 Discussion

In this study, we have presented an optimized CO_2 fire prior flux based on emission ratio between CO_2 and CO that comes from optimized CO fire emissions using MOPITT CO retrievals. In addition, as fire emissions and plant respiration (and hence

net fluxes terms included in the net fluxes) are difficult to disentangle a priori, we re-balanced the respiration with each fire prior and with the annual NOAA growth rate. We then explored a range of NEE emissions based on different fire emissions including a CO_2 fire estimate calculated from CO fire emissions information in order to better constrain biospheric emissions. We focused our study for the period 2015-2018 to observe the impact of the El Niño event in 2015 and the recovery period which followed it.

Globally, and for most regions, we find that the dependence of the inversion results on prior emissions is of secondary importance when compared with the data constraint, in the sense that variations in posterior flux are much smaller across different prior mean fluxes (and the different uncertainties that come from scaling the prior mean flux) as compared with differences resulting from assimilating OCO-2 versus in situ data. There are exceptions, most notably in the Northern and Southern Tropics, where the in situ constraint is especially limited and the corresponding posterior annual fluxes vary by as much as 0.5 PgC, which is a large fraction of the expected total El Niño signal. This suggests that in situ constrained flux estimates in the Tropics are more sensitive to the assumed prior flux, of which fires are a significant component, and should be assigned the appropriate amount of uncertainty in accordance with this finding. It also implies that while residual biases in satellite retrievals remain a key focus of the top-down inversion community, further work is needed to improve prior fluxes in Tropical regions as well as deploy more in situ measurements. Current efforts by multiple organizations should assist in that effort on a short time basis, but more investments in long term monitoring are needed (communication from Kathryn McKain). OCO-2 inversions are also sensitive to the prior assumption in Northern Africa, though to a lesser extent, as well as in Tropical Asia. Tropical Asia have been particularly well studied in the past where Nechita-banda2018 and VanderWerf2017 have shown the underestimation of GFED inventories over peat fires compared to space-based instruments such as IASI and MOPITT. This reinforces the need for better measurements and bottom up estimates of biospheric and fire fluxes in these Tropical regions. Nechita-Banda et al., (2018) converted their CO fire emissions in CO_2 emissions using emission factors and estimated that a range of 0.35-0.60 PgC was emitted in Indonesia and Papua from the 2015 fires. We calculated our fire CO_2 emissions over the same region and found 0.41 PgC, 0.37 PgC and 0.39 PgC for FIRE3, FIRE4 and FIREMo respectively. Our fire CO_2 estimates are hence in agreement with those found by Nechita-Banda et al., (2018). As mentioned previously, we know that GFED4.1s has information of small fires compared to GFED3 which allow better accuracy particularly over the Tropics where peat fires are important. However, we can see lower FIRE4 emissions than FIRE3 for southern tropical south Asia, similarly to what Shi et al., (2015) have found for the 2002-2012 period. A possible explanation could be that the CASA biogeochemical model of GFED3 predicts higher biomass densities than with the new version used in GFED4. Validation against fuel loads measured in savanna and grassland field have been found higher than with GFED4 (Randerson et al., (2012), Giglio et al., (2013)). In 2015, during the onset of the El Niño event which caused intense fires over Indonesia, the fire estimated from MOPITT CO emissions FIREMo are stronger than with GFED4 FIRE4 emissions but lower than GFED3 FIRE3 emissions. redAs mentioned previously, we know that GFED4.1s has information of small fires compared to GFED3 which allow better accuracy particularly over the Tropics where peat fires are important. Over Southern Tropical and Northern Tropical Asia, the combination of the spatio-temporal variability of MOPITT CO fire and the GFED4.1s emissions information included in the prior fire emissions of the CO inversion might bring additional information in the emission ratio and

hence in the fire prior used in CO_2 inversions. Indeed, fires over peat lands spread more during the El Niño event due to intense drought conditions (NechitaBanda2018). Consequently, they emit two to four times more CO than forest fires (Akagi2011) and contribute significantly to the exchange between terrestrial carbon stocks and the atmosphere by decreasing the uptake of atmospheric CO_2 by the biosphere. This is particularly shown for the IS inversions where IS4re and ISMore have sources of carbons compared to the IS constrained with the GFED3 fires, showing then higher net sources with GFED4 and MOPITT than with GFED3 fires. Moreover, the CO_2 posterior emissions using MOPITT CO information were able to catch the seasonality of fires over Southern tropical Asia during the El Niño event as discussed in NechitaBanda2018 and VanderLaan-Luijkx2015 that the other priors using GFED inventory were not able to capture. This is particularly shown for the IS inversions where IS4re and ISMore have higher net sources of carbons compared to the IS constrained with GFED3 fires. Moreover, FIREMo was able to catch the seasonality of fires over southern tropical Asia during the El Nino event, compared to the other priors using GFED inventory. As discussed in NechitaBanda et al., (2018) and van der Laan-Luijkx et al., (2015) for Equatorial Asia and tropical south America, GFED4 does not capture fire seasonality due to the use of burned area, compared to GFAS. In both GFED and GFAS method (and similarly for MOPITT), the detection of fires underneath clouds and below the canopy is difficult. But, FIREMO emissions, compared to FIRE3 and FIRE4, has the advantage of combining optimized fire emissions with local observations. It is thus important to use CO observations to constrain estimates of CO2 fire emissions, and subsequently constrain NEE with OCO-2 and IS observations But uncertainty in our emission ratio remains when converting CO to CO_2 emissions in our prior. GFED vegetation partition only account for six different types of vegetation which might not be fine enough to represent all different types of fuels. Additionally, the emission factors used in the emission ratio , lack spatial and temporal variability to account for the full dynamics range of combustion characteristics are characteristic of vegetation type but are not dependent of spatial or temporal scales. We know, for instance, that African savanna fires can go from flaming to smoldering, changing the combustion efficiency and then the gases emitted (Zheng2018a). This could explain the differences observed over some regions of the Tropics between the priors using CO fire emissions blueFIREMo and the other prior fire CO_2 emissions. Further works are needed is required to improve emission ratios and particularly emission factors over different spatial and temporal scales. A recent study has shown the underestimation for Africa of MODIS burned area and consequently GFED4s, compared to the new Sentinel-2 burned area product (Ramo et al., (2021)). The higher fire posterior emissions observed with previous studies using GFAS as a prior compared to GFED4 (Nechita-Banda et al., (2018)) and the results of Ramo et al., (2021) seems to suggest for future work to carefully choose the CO fire prior used in a CO-CO2 study. Future work will be done comparing different CO posterior emissions. However, the estimation of EF and consequently the emission ratio CO/CO_2 cannot be determined accurately in the field and can introduce systematic errors in the EF(CO_2) values that may well exceed 10%. One challenge is separation of the information between small fire inputs of CO_2 (and hence their detection) from large biospheric variability. Other difficulties come from the issue of variable background concentrations and from smoldering emissions that are not projected into the smoke plumes (Guyon2005, Burling2011, Yokelson2013).

The data used to constrain the inversions are very important as we were able to see the differences between OCO-2 and IS inversions over this tropical region where the source is about 0.4 PgC/yr higher with IS than with OCO-2. This bring us to the importance of data assimilated in the inversions but also about the priors used in the inversions regarding the different

sectors (fire and terrestrial emissions). The data used to constrain inversions is very important. We could see up to 0.4 PgC/yr differences between OCO-2 and IS inversions in tropical regions. This bring us to the importance of the data assimilated in the inversions but also about the priors used in the inversions concerning the different sectors (fire and terrestrial emissions).

The difference in partitioning of fluxes in latitude and longitude for the different data constraints is not a new observation, and fits the findings of the v7 OCO-2 MIP Crowell2019 and previous studies comparing GOSAT and in situ data (Reuter2014, Houweling2015a)) as well as of the v9 OCO-2 MIP, an extension of the v7 OCO-2 MIP (Peiro2022). More specifically, the OCO-2 data constrain a stronger Northern Extra-Tropical sink in concert with a strong tropical source, while the in situ data generally constrain a weaker Northern sink and neutral Tropical flux, or even a sink. While the Northern Extra-Tropics are relatively densely sampled by the in situ network, Schuh2019 found a strong sensitivity of flux estimates to model transport, particularly in the vertical and meridional transport of CO_2. Though we utilized only TM5 in these experiments, the findings here are consistent with those found in their study.

Within each zonal band, there are disparities in how the flux is partitioned, but these are again driven more strongly by data constraint than by prior. In the Northern Extra-Tropics, the partitioning of the sink across continents is more robust in the OCO-2 posterior results than IS, with both North America and North Asia accounting for a sink of 1-1.5 PgC and Europe a bit less. The IS results suggest a very strong sink in North Asia (< -1.5 PgC) relative to North America (-0.6 PgC with around 0.5 PgC of source in 2015) and Europe (-0.5 PgC to -0.1 PgC). When we look at the North Tropics, all inversions see a source in North Tropical South America, and this persists longer in the IS measurements into 2017 while ending sooner in the OCO-2 inversions. The largest difference is in North Tropical Africa, where OCO-2 sees a persistent source with varying magnitude, while IS fluxes depict a sink in 2015 and 2018 and near-neutral flux in 2016-2017. Given our current understanding of Africa's response to the El Niño from previous studies measurements (Gloor2018), strong sinks in Northern Africa are unlikely. Interestingly, IS fluxes imply a post El Niño recovery in the North Tropical Asia with net sources in 2015-2016 and sink of more than 0.4 PgC per year in 2017-2018, while OCO-2 sees a progressive transition and smaller response from -0.2 PgC/yr in 2016 through -0.4 PgC/yr in 2018. The Southern Tropics show most of the source activity from OCO-2 (southern tropical South America and southern tropical Asia), while again the IS data constrain a sink, except in Southern Tropical Asia.

Returning to the question of importance of the prior, it would seem that the simulation experiments in Philip2019 hold for our experiments as well, i.e. that OCO-2 inversions are relatively insensitive to the prior in most regions. Regarding the question of the importance of the prior and the question of which prior could do better than the others, we have seen through the results and the evaluation, than no simulation is better than the other on average. Even if the biases seem to have been reduced with FIREMO for certain sites (such as Ascension island for instance), they are in the same order as the other a priori biases for other site. On average and and overall, the added value of optimizing fire emissions before optimizing NEE is not very apparent. Our results seem, overall, to be very insensitive to optimized fire emissions. Philip et al., (2019) performed simulation experiments with different NEE priors, and concluded that posterior NEE estimates are insensitive to prior flux values. But they found large spread among posterior NEE estimates in regions with limited OCO-2 observations. Our results suggesting that OCO-2 inversions are relatively insensitive to prior in most regions, are consistent with Philip et al., (2019), and not only for OCO-2 inversions but also for IS inversions.

A generally accepted (though not documented) assertion is that a minimal amount of data is required to constrain the global growth rate, and yet we see here that OCO-2 and the global in situ network do not see the same global annual flux, even assuming the same transport and prior flux that matches the NOAA AGR. Certainly some of this mismatch is due to sampling differences, as most of the in situ measurements assimilated here are taken in the atmospheric boundary layer in the Northern Extra-Tropics, whereas OCO-2 measurements are globally distributed, but with seasonally varying coverage. Part of this discrepancy is certainly due to: (i) most of the in situ measurements assimilated here are taken in the atmospheric boundary layer while OCO-2 represents a column density; and (ii) most of the in situ measurements are in the northern extra-tropics, whereas OCO-2 measurements are globally distributed, but with seasonally varying coverage. Persistent transport biases as well as satellite retrieval errors likely play a factor in this global offset, though further investigation is necessary to assess the relative importance of each.

5 Conclusions

In this study, we have explored the potential of using CO/CO_2 emission ratio to add CO fire information in CO_2 inversions in order to better estimate and constrain CO_2 biospheric emissions. Fires have the potential to influence inter-annual variability and long-term trends in atmospheric CO_2 concentrations and particularly alter the seasonal cycle of net biome production. CO measurements are available with high precision from space and bring more accuracy in CO fire emission estimates. Including more accurate fire emissions in CO_2 inversions could improve the estimates of CO_2 land fluxes relative to a CO_2 inversion without the added information of CO. In this paper, we showed how we added on global scale CO/CO_2 emission ratio and its respective re-balanced respiration with fire and NEE with annual NOAA growth rate, and its value for CO_2 inversions.

We performed several CO_2 transport inversions assimilating separately OCO-2 data and in situ measurements from 2015 through 2018. We found that OCO-2 and in situ net fluxes have, even if with a difference, a better agreement at global scale as observations are dense enough to constrain the fluxes than at latitudinal and regional scale. Differences in net fluxes are particularly important over the Tropics not only between OCO-2 and in situ inversions but also between the different priors used. Discrepancies between in situ and OCO-2 inversions occurred over Northern Tropical Africa where OCO-2 inversions have shown net sources while in situ inversions have shown sinks. However, over Southern Tropical regions, discrepancies appear between the different set of priors, with higher net sources observed with the inversion using the CO/CO_2 emission ratio (MOre inversion) for OCO-2 inversion over Southern Tropical South America and with IS inversion over Southern Tropical Asia, compared to the IS inversions using GFED3 fires. For tropical Asia, the constrain of priors seems to be more important than the data assimilated. Additionally, over this region, seasonality from CO_2 inversions using MOPITT fires seems to be better representative of the large Indonesian fires that occurred during the 2015 El Niño event.

TCCON evaluation suggested that the prior using the FIREMo (CO_2 fire prior emissions computing using CO/CO_2 emission ratio) gives accuracy in CO_2 mixing ratio comparable to GFED4 but with slightly larger biases over the Northern Hemisphere and biases of the priors with the re-balanced respiration are smaller than the CMS prior. However, biases for the posterior simulated mixing ratio are in the same order. Evaluation mainly showed that biases have been decreased and variability matches

1015 better those of TCCON for the re-balanced posterior simulated mixing ratio suggesting the importance of the accuracy in fire priors and the re-balanced of terrestrial emission with fires for CO_2 posteriors emissions. The added value of fire emission for NEE optimization is not apparent. Our results seem hence to be very insensitive to optimized fire emissions.

We illustrated the potential of using CO/CO_2 emission ratio, and the re-balanced respiration and NEE with fire and growth rate, in CO_2 inversion for better constraint and accuracy in the CO_2 fire prior emissions and biospheric emissions estimates.
1020 We found that a priori CO_2 flux uncertainties are substantially reduced when matching the NOAA AGR as well as CO/CO_2 ratio but not strong enough compared to a re-balanced GFED and GFED4.1s NEE, and suggest hence for future work the development of joint CO-CO_2 inversions with multi-observations for stronger constraint in posterior CO_2 fire and biospheric emissions. We found that CO_2 fluxes are more robust if the NEE and fire emissions are rebalanced in order to match the NOAA AGR. However, a more reliable NEE is obtained with the assimilated data, using either in situ or satellite-based CO2
1025 constraints. This opens new avenues for future research for the development of a joint CO-CO2 inversion framework that uses multiple streams of data to improve the fire and biosphere emissions. Besides, the multi-species approach employing CO and CO_2 for instance is important for the interpretation of upcoming satellite data such as data from the future NASA Earth Venture Mission, GeoCarb.

Appendix A: GFED versions descriptions

The first version of GFED was released in 2004. Since then, several improvements have been incorporated into GFED. Improvement on the mapping of burned area from active fire data in GFED2 Giglio2006 was no longer necessary when the MODIS product became available for GFED3 Giglio2010. Burned area particularly affects the spatiotemporal variability of carbon emissions during fires. This spatiotemporal impact has been implemented in GFED with biogeochemical modeling framework providing estimation of biomass combustion over different vegetation types Giglio2013. All GFED versions are then based on the Carnegie-Ames-Standford Approach (CASA) model adjusted to account for fires (see VanderWerf2004 and VanderWerf2017 for more details). The most recent versions (GFED4 and GFED4.1s which includes small fire burned area) modified the burned-area-to-burned fraction conversion, which have been shown to increase burned area and fire carbon emissions with 11% in GFED4.1s compared to GFED3 vanderwerf2017 at the global scale. JCLiu2017 found that with the omission of small fires in GFED3, global fire emissions are underestimated. Accounting for small fires increased global burned area and carbon emissions by 35% Randerson2012, and improved the agreement of spatial distribution between active fires and burned area over regions with large fires such as savanna fires and boreal forests. Including small fires in GFED amplifies emissions over regions where drought stress and burned area varied considerably from year to year in response to, for instance, the El Niño Southern Oscillation (ENSO).

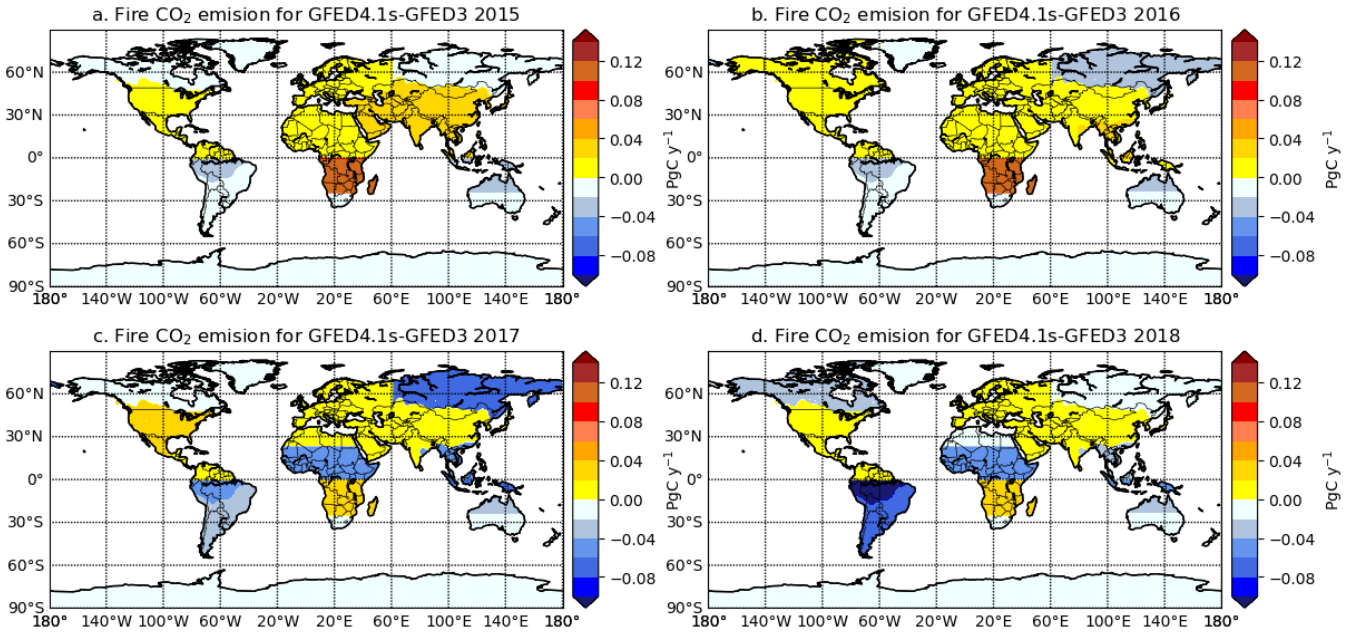

Figure A1. Annual differences between FIRE4 and FIRE3 in PgC/yr over the regions of Fig. 3 for a) 2015, b) 2016, c) 2017 and d) 2018.

Figure A1 shows annual differences between FIRE3 and FIRE4 from 2015 through 2018 over the OCO-2 MIP regions. We note that regional differences are as large as 140 TgC per year, or roughly ∼10% of the annual global fire emissions budget

which has been estimated to 1.6 $\pm$ 0.7 GtC/yr Friedlingstein2020. Additionally, the size and sign of the differences varies by year and by region. For instance, FIRE3 generally predicts higher CO_2 emissions over the Boreal regions, while FIRE4 (GFED4.1s) largely predicts more fire emissions from the Northern midlatitudes. This is consistent with differences between the two models, i.e. GFED4.1s uses a different set of emission factors separating trace gas emissions and aerosol from boreal forest to temperate forests Akagi2011, VanderWerf2017. VanderWerf2017 have shown that GFED3 does not capture the different patterns of fire severity between the boreal regions of North America and Eurasia and the differences between boreal and temperate forests fires (which could explain the large difference between FIRE4 and FIRE3 in Fig.A1). In addition, VanderWerf2017 found that including small fire burned area in GFED4 doubled the burned area in temperate North America and Europe compared to GFED3. Interestingly, the differences in the tropics have a pronounced zonal structure, where GFED4.1s predicts smaller emissions in south America, tropical Asia, and north Africa (after 2016), and larger emissions in southern tropical Africa. The addition of small fire burned area included in GFED4.1s has a strong impact in the southern tropical Africa regions where agricultural waste burning and shifting cultivation are important drivers of fire activity. VanderWerf2017 have shown that the increase of burned area in these regions were associated with small fire burned area from the last GFED version. Small fires linked with deforestation and agricultural waste are also important over the Indonesia, however deforestation activity decreased of almost 50% in 2017 and 2018 thanks to several Indonesian policies in order to prevent forest fires and land clearing with particularly the new law avoiding to clear forest for oil palm plantations GlobalForestWatch2020. This might explain the decrease in fire emissions over Southern Tropical Asia in 2017 and 2018 with GFED4.1s, in addition that 2017 and 2018 were not impacted by the 2015 El Niño event where large fires burned in Indonesia.

Author contributions. H.Peiro generated the CO products, MOPITT CO_2 fires and re-balanced priors, produced the figures and wrote the manuscript. S.Crowell generated the CO_2 products, provided comments and feedback on the manuscript. B.Moore provided feedback on the manuscript as well.

Competing interests. The authors declare that they have no conflict of interest.

Acknowledgements. We are thankful to Debra Wunch who helped us reviewing the TCCON references and acknowledgements, and to both Debra Wunch and Coleen Roehl who contacted the TCCON PIs. The TCCON data were obtained from the TCCON Data Archive hosted by CaltechDATA at https://tccondata.org. We thanks TCCON PIs for the TCCON measurements at Eureka, Ny-Ålesund, Sodankylä, Białystok, Bremen, Karlsruhe, Paris, Orléans, Garmisch, Park Falls, Rikubetsu, Lamont, Anmeyondo, Tsukuba, Edwards, Caltech, Saga, Izaña, Ascension Island, Darwin, Réunion Island, Wollongong, Lauder. Eureka measurements are made by the Canadian Network for the Detection of Atmospheric Change (CANDAC) and in part by the Canadian Arctic ACE Validation Campaigns. They are supported by the Atlantic Innovation Fund/Nova Scotia Research Innovation Trust, Canada Foundation for Innovation, Canadian Foundation for Climate and Atmospheric Sciences, Canadian Space Agency, Environment Canada, Government of Canada International Polar Year funding, Natural Sciences and Engineering Research Council, Northern Scientific Training Program, Ontario Innovation Trust, Ontario Research Fund and Polar Continental Shelf Program. Observations for Białystok are funded byt the European Union (EU) projects InGOS and ICOS-INWIRE, and bu the Senate of Bremen. Local support for Bremen and Ny-Ålesund are provided by the EU projects InGOS and ICOS-INWIRE (26188, 36677, 284274, 313169 and 640276), and by the Senate of Bremen. Orléans observations are supported by the EU projects InGOS and ICOS-INWIRE, by the Senate of Bremen and by the RAMCES team at LSCE. The Réunion Island TCCON site is operated by the Royal Belgian Institute for Space Aeronomy with financial support since 2014 by the EU project ICOS-Inwire and the ministerial decree for ICOS (FR/35/IC1 to FR/35/IC5) and local activities supported by LACy/UMR8105 – Université de La Réunion. The Paris TCCON site has received funding from Sorbonne Université, the French research center CNRS, the French space agency CNES, and Région Île-de-France. Garmisch funding was provided by the EC within the INGOS project. Park Falls, Lamont, Edwards and Caltech TCCON site have received funding from National Aeronautics and Space Administration (NASA) grants NNX14AI60G, NNX11AG01G, NAG5-12247, NNG05-GD07G, and NASA Orbiting Carbon Observatory Program. They are supported in part by the OCO-2 project. The TCCON station at Rikubetsu and Tsukuba are supported in part by the GOSAT series project. Darwin and Wollongong TCCON stations are funded by NASA grants NAG5-12247 and NNG05-GD07G and supported by the Australian Research Council (ARC) grants DP140101552, DP110103118, DP0879468 and LP0562346. Lauder TCCON site has received funding from National Institute of Water and Atmospheric (NIWA) Research through New Zealand's Ministry of Business, Innovation and Employment. We also acknowledge the ObsPack data used for our IS inversions.